

RESEARCH ARTICLE SUMMARY

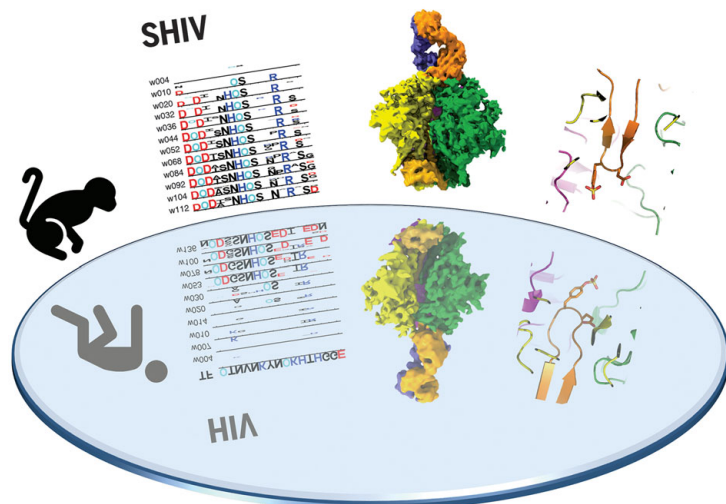
HIV

Recapitulation of HIV-1 Env-antibody coevolution in macaques leading to neutralization breadth

Ryan S. Roark*, Hui Li*, Wilton B. Williams*, Hema Chug*, Rosemarie D. Mason*, Jason Gorman*, Shuyi Wang, Fang-Hua Lee, Juliette Rando, Mattia Bonsignori, Kwan-Ki Hwang, Kevin O. Saunders, Kevin Wiehe, M. Anthony Moody, Peter T. Hraber, Kshitij Wagh, Elena E. Giorgi, Ronnie M. Russell, Frederic Bibollet-Ruche, Weimin Liu, Jesse Connell, Andrew G. Smith, Julia DeVoto, Alexander I. Murphy, Jessica Smith, Wenge Ding, Chengyan Zhao, Neha Chohan, Maho Okumura, Christina Rosario, Yu Ding, Emily Lindemuth, Anya M. Bauer, Katharine J. Bar, David Ambrozak, Cara W. Chao, Gwo-Yu Chuang, Hui Geng, Bob C. Lin, Mark K. Louder, Richard Nguyen, Baoshan Zhang, Mark G. Lewis, Donald D. Raymond, Nicole A. Doria-Rose, Chaim A. Schramm, Daniel C. Douek, Mario Roederer, Thomas B. Kepler, Garnett Kelsoe, John R. Mascola, Peter D. Kwong, Bette T. Korber, Stephen C. Harrison, Barton F. Haynes, Beatrice H. Hahn, George M. Shaw†

INTRODUCTION: It is widely believed that the development of an effective neutralizing antibody-based HIV-1 vaccine will require consistent activation of multiple germline precursor B cells that express immunoglobulin receptors specific for one or more of the canonical broadly neutralizing antibody (bNAb) epitope clusters, followed by efficient antigen-driven selection for antibody affinity maturation. How to accomplish this feat by immunization has proven to be a daunting scientific challenge. One roadblock to rational HIV-1 vaccine design is the lack of a suitable outbred primate model in which bNAbs can be commonly induced, thereby enabling the molecular, biological, and immunological mechanisms responsible for such responses to be studied in a reproducible and iterative fashion.

RATIONALE: Given that most HIV-1 bNAbs identified to date have come from humans chronically infected by HIV-1, we hypothesized that one means to elicit such antibodies in primates might be by infecting rhesus macaques (RMs) with simian-human immunodeficiency virus (SHIV) strains that bear primary HIV-1 envelope proteins (Envs), including those that induced bNAbs in humans. SHIV-infected RMs could then be used to assess the potential of particular HIV-1 Envs to elicit bNAbs and to characterize the coevolutionary pathways of bNAb lineages and the cognate Env intermediates that elicited them, thus serving as a molecular guide for rational vaccine design. Recent innovations in SHIV design make this experimental strategy testable.



Envelope-antibody coevolution in monkey and human. Env-antibody coevolution in SHIV-infected rhesus macaques mirrors that in HIV-1-infected humans, including the elicitation of broadly neutralizing antibodies. The illustration depicts a mirror with images, left to right, of organism, longitudinal changes in viral Env sequence, Env trimer recognition by virus-elicited broadly neutralizing antibodies, and atomic-level details of paratope-epitope interactions.

RESULTS: Neutralizing antibodies elicited by HIV-1 in naturally infected humans coevolve with viral Envs in distinctive molecular patterns, in some cases acquiring substantial breadth. We constructed SHIVs bearing primary transmitted/founder Envs from three HIV-1 infected humans who developed bNAbs and used these SHIVs to infect 22 RMs. Seven monkeys developed bNAbs that exhibited a wide range of breadth and potency. Unexpectedly, SHIV infections elicited molecular patterns of Env-antibody coevolution in monkeys that mirrored what was seen in humans infected by HIV-1 strains bearing homologous Envs. Similarities included conserved immunogenetic, structural, and chemical solutions to epitope recognition and precise Env-amino acid substitutions, insertions, and deletions leading to virus persistence. One rhesus antibody, capable of neutralizing 49% of a 208-strain global virus panel, contained a 24-amino acid heavy chain complementarity-determining region 3 (HCDR3) with a sulfated tyrosine at its tip; this rhesus bNAb exhibited a V2 apex mode of recognition similar to human bNAbs PGT145 and PCT64-35S, with critical interactions involving lysine or arginine residues at Env positions 121, 166, and 169 and an N-linked glycan at position 160. Another rhesus antibody bound the CD4 binding site by CD4 mimicry mirroring human bNAbs 8ANC131, CH235, and VRC01. In other SHIV-infected animals, bNAb responses targeted a canonical V3 high mannose patch epitope cluster that included Env residues ³²⁴GDIR³²⁷ and N332. Molecular patterns of epitope evolution enabling virus escape, and at the same time promoting bNAb affinity maturation, were similar in SHIV-infected RMs and HIV-1-infected humans.

CONCLUSION: SHIV infection of RMs is the only model system other than naturally infected humans where the immunogen (Env) coevolves with neutralizing antibodies. The high mutability and dynamic replication of HIV-1 and SHIV in vivo result in a constantly evolving virus quasispecies, which means that Envs with binding affinities sufficient to drive bNAb lineage affinity maturation are continuously being generated. SHIV-infected macaques may thus provide insights for vaccine design by enabling the identification of Env intermediates that can guide the evolution of precursor B cells through stages of affinity maturation leading to breadth and potency. ■

The list of author affiliations is available in the full article online.

*These authors contributed equally to this work.

†Corresponding author. Email: shawg@penncmedicine.upenn.edu

Cite this article as R. S. Roark *et al.*, *Science* **371**, eabd2638 (2021). DOI: 10.1126/science.abd2638

S READ THE FULL ARTICLE AT
<https://doi.org/10.1126/science.abd2638>

RESEARCH ARTICLE

HIV

Recapitulation of HIV-1 Env-antibody coevolution in macaques leading to neutralization breadth

Ryan S. Roark^{1*}, Hui Li^{1*}, Wilton B. Williams^{2,3*}, Hema Chug^{4*}, Rosemarie D. Mason^{5*}, Jason Gorman^{5*}, Shuyi Wang¹, Fang-Hua Lee¹, Juliette Rando¹, Mattia Bonsignori^{2,3}, Kwan-Ki Hwang², Kevin O. Saunders^{2,6}, Kevin Wiehe^{2,3}, M. Anthony Moody^{2,7}, Peter T. Hraber⁸, Kshitij Wagh⁸, Elena E. Giorgi⁸, Ronnie M. Russell¹, Frederic Bibollet-Ruche¹, Weimin Liu¹, Jesse Connell¹, Andrew G. Smith¹, Julia DeVoto¹, Alexander I. Murphy¹, Jessica Smith¹, Wenge Ding¹, Chengyan Zhao¹, Neha Chohan¹, Maho Okumura¹, Christina Rosario¹, Yu Ding¹, Emily Lindemuth¹, Anya M. Bauer¹, Katharine J. Bar¹, David Ambrozak⁵, Cara W. Chao⁵, Gwo-Yu Chuang⁵, Hui Geng⁵, Bob C. Lin⁵, Mark K. Louder⁵, Richard Nguyen⁵, Baoshan Zhang⁵, Mark G. Lewis⁹, Donald D. Raymond⁴, Nicole A. Doria-Rose⁵, Chaim A. Schramm⁵, Daniel C. Douek⁵, Mario Roederer⁵, Thomas B. Kepler^{10,11}, Garnett Kelsoe^{2,6}, John R. Mascola⁵, Peter D. Kwong⁵, Bette T. Korber⁸, Stephen C. Harrison^{4,12}, Barton F. Haynes^{2,3}, Beatrice H. Hahn¹, George M. Shaw^{1†}

Neutralizing antibodies elicited by HIV-1 coevolve with viral envelope proteins (Env) in distinctive patterns, in some cases acquiring substantial breadth. We report that primary HIV-1 envelope proteins—when expressed by simian-human immunodeficiency viruses in rhesus macaques—elicited patterns of Env-antibody coevolution very similar to those in humans, including conserved immunogenetic, structural, and chemical solutions to epitope recognition and precise Env–amino acid substitutions, insertions, and deletions leading to virus persistence. The structure of one rhesus antibody, capable of neutralizing 49% of a 208-strain panel, revealed a V2 apex mode of recognition like that of human broadly neutralizing antibodies (bNAbs) PGT145 and PCT64-35S. Another rhesus antibody bound the CD4 binding site by CD4 mimicry, mirroring human bNAbs 8ANC131, CH235, and VRC01. Virus-antibody coevolution in macaques can thus recapitulate developmental features of human bNAbs, thereby guiding HIV-1 immunogen design.

A major roadblock to rational HIV-1 vaccine design is the lack of a suitable primate model in which broadly neutralizing antibodies (bNAbs) can be commonly induced and the molecular, biological, and immunological mechanisms responsible for such responses studied in a reproducible and iterative fashion. Because most HIV-1 bNAbs identified to date have come from humans chronically infected by HIV-1, we hypothesized that one means to elicit such antibodies in primates might be by infecting Indian rhesus macaques

(RMs) with simian-human immunodeficiency virus (SHIV) strains that bear primary or transmitted/founder (T/F) HIV-1 envelope proteins (Envs) that induced bNAbs in humans (1–7). SHIV-infected RMs could then be used to assess the potential of particular HIV-1 Envs to elicit bNAbs and to characterize the coevolutionary pathways of bNAb lineages and the cognate Env intermediates that elicited them (2–8), thereby serving as a molecular guide for rational vaccine design. Recent innovations in SHIV design (9) now make this experimental strategy testable.

HIV-1 bNAbs target one of several conserved regions on the native Env trimer, including the CD4 binding site (CD4bs), V2 apex, V3 high-mannose patch, glycoprotein gp120–gp41 interface, fusion peptide, glycosylated silent face, and membrane-proximal external region (10, 11). Such antibodies generally share certain features, such as exceptional heavy chain complementarity-determining region 3 (HCDR3) length, extensive somatic hypermutation, auto-reactivity, or unusual mechanisms for binding glycans or glycopeptides (10–13). Long HCDR3s result from initial germline immunoglobulin gene rearrangements, whereas the characteristic high frequencies of V(D)J mutations that lead to affinity maturation and neutralizing breadth result from persistent virus replication,

epitope variation, and continued Env-Ab coevolution. In some subjects, cooperating antibody lineages that target the same epitope have been identified, and together they contribute to Env diversification and bNAb development (4, 6). A critical question in the HIV-1 vaccine field is whether the relatively rare examples of high-titer bNAbs that have been identified in a subset of chronically infected humans represent stochastic accidents of nature, not likely to be replicated by a vaccine, or whether there are special properties of particular HIV-1 Envs that, along with deterministic features of Env-Ab coevolution, make HIV-1 vaccine development more plausible.

This study is based on the premise that while Env diversity within HIV-1 group M is extraordinarily high, primary HIV-1 Envs [that is, native Env trimers on infectious virions that allow for persistent replication and clinical transmission in humans (1)] are nonetheless constrained in their immediate evolutionary potential (14–16). This paradox—extreme Env diversity globally but constraints on immediate or near-term evolution in an individual—can be explained by competing evolutionary forces: positive selection imposed by immune evasion, balanced by purifying (negative) selection acting to retain viral fitness. At least four interrelated Env properties, acting in concert, facilitate immune escape—occlusion of trimer-interface epitopes (17), glycan shielding (18), epitope variation (19), and conformational masking (20)—while conservation of structure and cell-entry properties and retention of protein stability constrain each primary Env's immediate and short-term evolutionary trajectory. When introduced into a human as HIV-1 infection or into RMs as SHIV infection, each Env will have distinctive restrictions in its exposure of antigenic sites, thus favoring distinct molecular pathways of escape from neutralizing antibodies with each pathway exacting a different fitness cost from the virus. These considerations led us to hypothesize that SHIV infection of RMs will recapitulate HIV-1 infection of humans with respect to molecular patterns of Env-Ab coevolution, within the bounds set by any particular Env sequence and the respective rhesus and human immunoglobulin gene repertoires that respond to it (21).

Some of the best-studied examples of HIV-1 Env-Ab coevolution have come from the analysis of HIV-1-infected human subjects CH505, CH848, and CAP256, who developed bNAb responses targeting the CD4bs, V3 high-mannose patch, and V2 apex of HIV-1 Env, respectively (2–7). Subjects CH505 and CH848 were each productively infected by a single T/F virus, and we previously constructed SHIVs containing each of these T/F Envs (9). Subject CAP256 was infected by a single virus (CAP256PI, primary infection) and then became superinfected by a second genetically divergent virus (CAP256SU,

¹Departments of Medicine and Microbiology, Perelman School of Medicine, University of Pennsylvania, Philadelphia, PA 19104, USA. ²Duke Human Vaccine Institute, Duke University School of Medicine, Durham, NC 27710, USA. ³Department of Medicine, Duke University School of Medicine, Durham, NC 27710, USA. ⁴Laboratory of Molecular Medicine, Boston Children's Hospital and Harvard Medical School, Boston, MA 02115, USA. ⁵Vaccine Research Center, National Institute of Allergy and Infectious Diseases, National Institutes of Health, Bethesda, MD 20892, USA. ⁶Departments of Immunology and Surgery, Duke University School of Medicine, Durham, NC 27710, USA. ⁷Departments of Pediatrics and Immunology, Duke University School of Medicine, Durham, NC 27710, USA. ⁸Theoretical Biology and Biophysics, Los Alamos National Laboratory, Los Alamos, NM 87545, USA. ⁹Bioqual, Inc., Rockville, MD 20850, USA. ¹⁰Department of Microbiology, Boston University School of Medicine, Boston, MA 02118, USA. ¹¹Department of Mathematics and Statistics, Boston University, Boston, MA 02215, USA. ¹²Howard Hughes Medical Institute, Harvard Medical School, Boston, MA 02115, USA.

*These authors contributed equally to this work.

†Corresponding author. Email: shawg@penmedicine.upenn.edu

superinfection) (22). The CAP256SU variant was thought to trigger the V2 bNAb lineage in this individual (5), so we constructed and analyzed a SHIV containing this Env (fig. S1). SHIVs containing CH505, CH848, and CAP256SU Envs were modified at gp120 residue 375 to enhance binding and entry into rhesus CD4 T cells. The Env375 substitutions resulted in no discernible change in antigenicity or sensitivity to anti-HIV-1 NAb compared with wild-type virus, but they were essential for replication in primary RM CD4⁺ T cells (fig. S1) (9). We inoculated 22 RMs (table S1) with SHIV.CH505 ($n = 10$), SHIV.CH848 ($n = 6$), or SHIV.CAP256SU ($n = 6$) by the intravenous route and followed them for an average period of 2 years (mean of 103 weeks, range 36 to 184 weeks) for viral replication kinetics, development of strain-specific (autologous) and broadly reactive (heterologous) NAb, and patterns of Env sequence evolution. Eight of the animals were treated with anti-CD8 monoclonal antibody (mAb) at or near the time of SHIV inoculation to transiently deplete CD8⁺ cells and increase peak and set point plasma virus titers. One animal (RM5695), which was repurposed from an earlier study of HIV-1 gp120 protein immunization (23), was inoculated with plasma from three animals recently infected by SHIV.CH505 to increase early virus diversity.

SHIV replication in vivo and elicitation of NAb

Figure S2 depicts the kinetics of virus replication and the development of autologous, strain-specific tier 2 NAb as measured by plasma viral RNA (vRNA) and inhibition of virus entry into TZM-bl cells (18). Acute virus replication kinetics were consistent for all SHIVs in all animals with peak viremia occurring about 14 days after inoculation and reaching titers in the 10^5 to 10^8 vRNA/ml range [geometric mean (GM) = 4.2×10^6]. Peak vRNA titers were higher in anti-CD8 treated animals than in untreated animals [geometric mean titers (GMT) of 2.6×10^7 versus 1.5×10^6 , respectively; $P < 0.0001$]. Plasma virus load set points at 24 weeks after infection varied widely, between 100 and 988,110 vRNA/ml, with a mean for anti-CD8 treated animals of $248,313 \pm 136,660$ vRNA/ml compared with 8313 ± 3509 vRNA/ml for untreated animals ($P = 0.002$). Set point vRNA levels in human subjects infected with the corresponding HIV-1 CH505, CH848, or CAP256 strains were 81,968, 132,481, and 750,000 vRNA/ml, respectively. Compared with two human cohort studies of acute and early HIV-1 infection (24, 25), peak and set point vRNA titers in SHIV-infected animals were comparable, although several macaques developed viral loads near the lower limit of detection (100 vRNA/ml), which is rare in humans. Six macaques developed AIDS-defining events and were euthanized at 36, 40,

60, 65, 89, or 136 weeks after SHIV infection; four of these animals had been treated with anti-CD8 mAb (table S1).

Autologous tier 2 NAb responses to the three SHIVs were detected as early as 8 weeks after infection and peaked between 24 and 80 weeks, with 50% inhibitory dilutions (ID_{50}) between 0.05 (1:20 dilution) and 0.000125 (1:8000 dilution) (fig. S2). The kinetics of appearance and titers of autologous tier 2 NAb that developed in response to SHIV infections were generally comparable to those observed in humans infected by viruses bearing the homologous Envs (2, 7, 22). Among all animals, there was a significant association between higher set point virus titers and higher autologous tier 2 NAb titers (Spearman correlation rank correlation coefficient $r_s = 0.74$, $P < 0.0001$).

Heterologous plasma neutralizing activity was assessed against a diverse 22-member global panel of tier 1a ($n = 3$) or tier 2 ($n = 19$) HIV-1 strains (26–29) (table S2). All animals developed potent neutralizing responses to the three tier 1a viruses (GMT $ID_{50} = 0.0004$). Tier 1a viruses have “open” Env trimers that spontaneously expose linear V3 and conformational CD4-induced (CD4i) bridging sheet epitopes, thus explaining their extreme sensitivity to what are otherwise non-neutralizing antibodies. Such non-neutralizing antibodies that target linear V3 and CD4i epitopes are elicited in virtually all HIV-1-infected humans, thereby selecting for Envs with an open-closed equilibrium that strongly favors the closed configuration (20, 30–32). Tier 2 viruses typify primary or T/F viruses that are generally resistant to neutralization by heterologous plasma antibodies except for those that target one of the canonical bNAb epitope clusters (1, 10, 11, 26). In this study, we used a reciprocal neutralization titer cutoff of $ID_{50} \leq 0.05$ against $\geq 33\%$ of heterologous tier 2 viruses as an indication of neutralization breadth. This is a conservative threshold consistent with other studies that have characterized bNAb prevalence in human cohorts (28, 33, 34).

Seven of 22 RMs developed antibody responses that neutralized between 6 and 18 of 18 heterologous HIV-1 tier 2 viruses in our test panel (Fig. 1A and table S2). Heterologous neutralization was first detected as early as 8 to 16 weeks after SHIV infection in two animals and as late as 88 weeks after SHIV infection in others. Heterologous NAb reached ID_{50} titers as high as 0.0001, with GMTs in the seven animals ranging from 0.018 (1:55) to 0.004 (1:271) (Fig. 1A). Peak and set point plasma virus titers were higher in the seven animals that developed bNAb (GMT = 18,150,586 and 47,471 vRNA/ml, respectively) than in animals that did not (GMT = 2,101,814 and 1945 vRNA/ml, respectively; $P < 0.015$ for both). Two animals with bNAb (RM5695 and RM6070) were infected by SHIV.CH505, two (RM6163 and RM6167) by

SHIV.CH848, and three (RM40591, RM42056, and RM6727) by SHIV.CAP256SU. The remaining 15 animals in the study showed either no or very limited, low-titer neutralization of heterologous tier 2 viruses (table S2). Altogether, the findings show that SHIVs bearing primary T/F Envs reproduce in RMs key features of virus replication dynamics and NAb elicitation that are characteristic of HIV-1 infection in humans, including the potential to elicit bNAb.

Figure 1B highlights the kinetics, potency, and breadth of neutralization by plasma from the SHIV.CH505-infected animal RM5695 and identifies immunoglobulin G (IgG) as the active component. By 16 weeks after infection, an autologous NAb response to SHIV.CH505 was detectable at an ID_{50} titer of 0.02 along with heterologous responses to viruses bearing HIV-1 25710, X1632, Q23, ZM233, T250, and WITO Envs at titers of 0.05 to 0.01. NAb increased rapidly in breadth and titer thereafter. By week 48, bNAb targeting Q23 and T250 jumped in titer to between 0.0002 and 0.0005 and against X1632, 246F3, ZM233, and WITO to titers of 0.005. By week 56, bNAb in the plasma of RM5695 neutralized 17 of 18 viruses in the heterologous HIV-1 test panel at titers ranging from 0.05 to 0.0002, along with a divergent tier 2 simian immunodeficiency virus strain (SIVcpz.MT145.Q171K) that shares selective antigenic cross-reactivity with HIV-1 in the V2 apex bNAb epitope cluster (35) at a titer of 0.006. IgG was purified from RM5695 week 56 plasma and assayed for neutralizing activity against the same 19 heterologous viruses: IgG concentrations between 0.002 mg/ml (corresponding to an ~1:10,000 dilution of rhesus plasma) and 4 mg/ml neutralized 18 of the 19 viruses in a rank order similar to the polyclonal plasma (Fig. 1B, far right panels). Neither plasma nor purified IgG neutralized control viruses pseudotyped with the murine leukemia virus (MLV) Env. Thus, anti-HIV-1-specific IgG accounted for all of the autologous and heterologous neutralizing activity in the RM5695 plasma. Of note, RM5695 plasma and plasma IgG from week 56 reached ID_{90} or ID_{95} thresholds against most viruses and exhibited steep inflections at the ID_{50} midpoint, indicating potent neutralization. Neutralization breadth detected as early as 16 weeks after infection is unusual in HIV-1 infection but not unprecedented (36) and occurs most often with V2 apex bNAb, likely because their activity depends more on long HCDR3s than on extensive somatic hypermutation. We show below that the bNAb activity in RM5695 plasma and its isolated IgG fraction as well as monoclonal bNAb derived from RM5695 all targeted a bNAb epitope in the V2 apex that included the conserved lysine rich C-strand and N160 glycan. The kinetics of appearance, breadth, titers, and potency of bNAb elicited in the six other SHIV-infected RMs, including three animals (RM6070, RM40591,

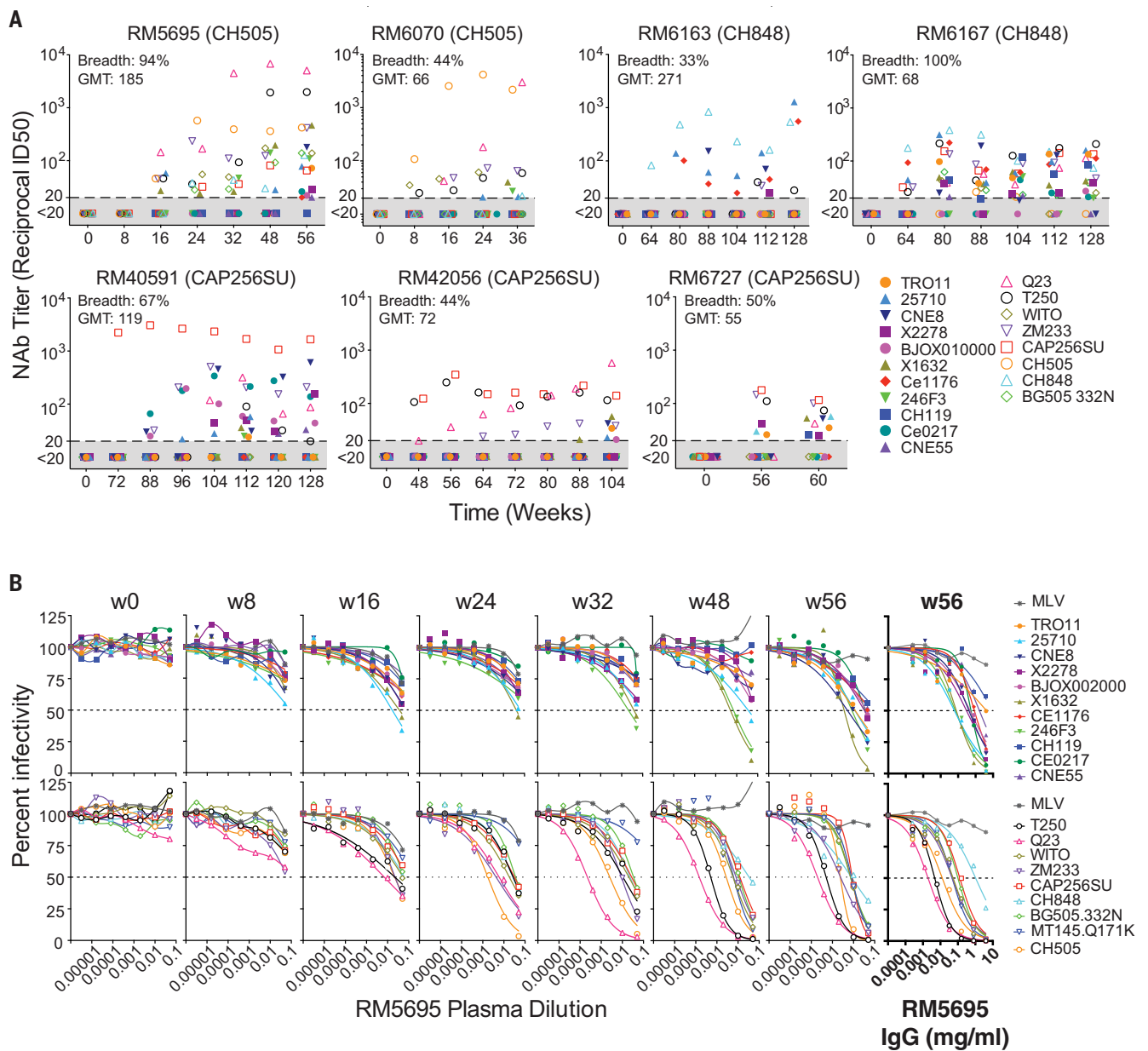


Fig. 1. Broadly neutralizing antibodies in seven rhesus macaques. (A) RMs 5695 and 6070 were infected by SHIV.CH505; RMs 6163 and 6167 by SHIV.CH848; and RMs 40591, 42056, and 6727 by SHIV.CAP256SU. Neutralizing antibody titers (ID_{50} , 50% inhibitory dilution) from longitudinal plasma specimens against 19 global tier 2 HIV-1 strains (26, 27, 84) are depicted. Full designations of target viruses are provided in fig. S22 and table S3. Maximum neutralization breadth across all time points and maximum geometric mean

titer (GMT) of neutralization at any one time point are indicated for each animal. (B) Neutralization curves for longitudinal plasma specimens and purified plasma IgG (highlighted in bold) from RM5695 show the development of broad and potent neutralization. MT145K.Q171K is a chimpanzee-derived SIVcpz strain that shares antigenic cross-reactivity with HIV-1 in the V2 apex (35, 131). Dashed lines indicate 50% reduction in virus infectivity. MLV, murine leukemia virus.

and RM42056) whose bNAbs also targeted the V2 apex C-strand, are summarized in Fig. 1A and table S2.

Env evolution in SHIV-infected macaques and HIV-1-infected humans

To explore whether SHIV Env evolution in RMs recapitulates that of HIV-1 in humans in a strain-specific manner, we analyzed Env sequences in the 22 SHIV-infected animals over

1 to 3 years of follow-up and compared them with the evolution of the homologous Envs in humans infected by HIV-1. We used single genome sequencing for this analysis, because it allows for retention of genetic linkage across intact viral genes and enables precise molecular tracking of sequence diversification from unambiguous T/F genomes (1, 37–39). We analyzed cDNA sequences derived from plasma virion RNA, because the half-life of circulating

plasma virus is <1 hour (40) and that of cells producing most of this virus is <1 day (40). This short composite half-life (<1 day) reflects the life span of >99.9% of circulating plasma virus in individuals not receiving antiretroviral therapy (41, 42), making the genetic composition of the plasma virus quasi-species an exquisitely sensitive real-time indicator of in vivo selection pressures acting on virus and virus-producing cells, including that exerted

Fig. 2. Env evolution in SHIV.CH505-infected rhesus macaques recapitulates HIV-1 Env evolution in human subject CH505. (A) A pixel plot (www.hiv.lanl.gov/content/sequence/pixel/pixel.html; www.hiv.lanl.gov/content/sequence/HIV/HIVTools.html) of amino acid alignments of longitudinal HIV-1 Env sequences obtained by single genome sequencing of plasma virion RNA. Between 15 and 60 individual sequences are grouped by time point, and amino acids are colored red to highlight mutations relative to the infecting CH505 transmitted/founder strain illustrated schematically at the top. The image is highly compressed. Each row within a time block represents a single sequence, and each column represents an amino acid position in the alignment; thus each pixel represents a single amino acid that is colored gray if it matches the T/F sequence, red if it is a mutated residue, and black if it is an insertion or deletion (indel) relative to the T/F virus. All SHIV sequences differ from the T/F at position 375, reflecting the SHIV design strategy that enables replication in rhesus macaques (9). Green tags indicate amino positions (HXB2 numbering) that are mutated in both human and rhesus. Yellow tags indicate three sites of identical indels observed in both human and rhesus. (B) LASSIE analysis (44) of the same longitudinal Env sequences was used to characterize mutations under positive selection. If a T/F amino acid was retained in <25% of the sequences in human CH505 infection, the site was considered to be under selective pressure and tracked in all hosts. The height of each amino acid mutation is proportional to its frequency at the respective time point. Red, dark blue, and black indicate

acidic, basic, and neutral residues, respectively. "O" indicates asparagine (N) embedded in an N-linked glycosylation motif. Numbers at the bottom indicate residue positions (HXB2 numbering). Green numbers indicate mutations that reached 75% frequency in the human and in at least one animal. (C) Side projection of the CH505 Env trimer with potential N-linked glycans (PNGs) indicated in blue, 10-Å neighbors of PNGs shown in green, and "glycan holes" that are typically covered by glycans in >80% and 50 to 80% of group M HIV-1 strains in magenta and pink, respectively. The light gray area in the central region of the trimer is the interprotomer surface that forms a cleft with low glycan coverage (45). Two glycan holes in the CH505 T/F at positions 234 and 332 were filled by the addition of NXS/T motifs over time in human subject CH505 and in RM6072 as well as in all other monkeys (see fig. S3). (D) The V1 sequence of CH505 env is shown at the top of the panel with the hypervariable region indicated in red. Indels in V1 that arose in the first year of infection in the human host are illustrated in the sequences below the reference T/F sequence. Indels occurred in nucleotide lengths divisible by three so as to maintain a viable Env open reading frame, and in the case of insertions, consisted of direct repeats. Indels that were replicated identically in one or more rhesus macaques are indicated by color-matched boxes to the right. Identical indels in human and rhesus CH505 sequences were also found in V4 and V5 (fig. S9). Single-letter abbreviations for the amino acid residues are as follows: A, Ala; C, Cys; D, Asp; E, Glu; F, Phe; G, Gly; H, His; I, Ile; K, Lys; L, Leu; M, Met; N, Asn; P, Pro; Q, Gln; R, Arg; S, Ser; T, Thr; V, Val; W, Trp; and Y, Tyr.

by NAb, cytotoxic T cells (CTLs), or anti-retroviral drugs (18, 37, 39, 42, 43). Figure 2A illustrates Env amino acid substitutions in virus from sequential plasma specimens from human subject CH505 and from six SHIV.CH505-infected RMs. By inspection and the algorithm-based statistical methods previously described [(37, 38) and supplementary materials], amino acid substitutions in Env were found to be nonrandomly distributed in patterns that evolved over time beginning as early as 4 weeks after infection. Using LASSIE (Longitudinal Antigenic Sequences and Sites from Intra-Host Evolution) (44), a computational tool that systematically identifies amino acid differences in a set of evolved sequences that reach a predetermined frequency threshold compared with a founder sequence, we identified in human subject CH505 15 Env residues where mutations altered the encoded amino acid in at least 75% of sequences at one or more subsequent time points. Thirteen of these 15 sites varied by >75% in one or more monkeys, and 10 sites varied in at least half of the animals (Fig. 2B). A highly parallel Env evolutionary trajectory was observed between the human host and monkey RM6072. Unexpectedly, the substituted amino acids at many of the variable sites were identical in human and rhesus sequences, including mutations that created potential N-linked glycans (PNGs) that filled "glycan holes" (Fig. 2C and fig. S3) (45). The conserved patterns of amino acid substitutions in CH505 Envs were very different from mutational patterns of Env sequences observed in the human subject CH848 and in RMs infected by SHIVs bearing the CH848 Env (fig. S4). Twenty-nine variable sites were identified in Envs from the human subject CH848, and 16 of these were shared in SHIV.

CH848-infected RMs, often with identical amino acid substitutions, including some that altered the distribution of PNGs and glycan holes (fig. S5). As a control, we compared patterns of Env evolution in CH848-infected RMs against selected sites in the CH505-infected human and vice versa. Many fewer sites of shared evolution were observed in both discordant Env pairings ($P < 0.01$ for both comparisons) (fig. S6). The Env strain-specific mutational patterns observed in humans and rhesus animals infected by CH505 and CH848 viruses were different still from the CAP256SU infected RMs in which 45 selected sites were identified, including 25 that were shared in more than one animal (figs. S7, A and B, and S8). A comparable Env-wide analysis in the human subject CAP256 could not be performed because this individual was infected and then superinfected by two widely divergent viruses whose progeny underwent extensive recombination (22) (fig. S7C). Still, we could identify common sites of positive selection in human and rhesus sequences, including a key mutation at residue 169 that led to virus escape from V2 apex C-strand targeted bNAbs (fig. S7D). Overall, we identified 89 selected Env residues in CH505, CH848, or CAP256SU T/F viruses, and 50 of these sites were shared among humans and RMs that were infected by viruses bearing the same Env strain. This result was markedly different for individuals infected by different virus strains where no more than 6 of these 89 variable sites were shared by any CH505, CH848, or CAP256SU pairing ($P < 0.0001$), and only 14 sites were shared overall ($P < 0.0001$). These findings thus show distinctive examples of conserved strain-specific evolution of HIV-1 Env sequences in humans and RMs.

Another type of Env variation common in HIV-1 infection that can affect immune recognition results from insertions and deletions (indels). Indels occur as a consequence of polymerase slippage and template switching during reverse transcription of the retroviral genome (46, 47). Indels are most commonly observed in the surface-exposed variable loops 1, 2, 4, and 5, which can better accommodate changes in sequence length than structural or enzymatic elements of the viral proteome; this was the case for human subject CH505 and macaques infected by SHIV.CH505 (Fig. 2A). Notably, we found multiple examples of identical indels between human and rhesus CH505 sequences and among CH505 sequences from different RMs (Fig. 2D and fig. S9). A total of six distinct V1 indels, three V4 indels, and one V5 indel were identified in sequences from human subject CH505 that were replicated exactly in sequences from one or more monkeys. Two of these indels were found in the human and in all six monkeys. Additional identically replicated indels in V1 and V5 were identified only in monkeys. Indels were also observed in sequences from human subject CH848 (figs. S4 and S10). An exact replica of all but one of these indels was present in one or more macaques. Additional indels were replicated in multiple animals (fig. S10). None of the indels in CH505 sequences were found in CH848, and neither set was found in CAP256SU sequences. In both human and rhesus, indels generally lengthened or shortened variable loops in a direction that approached the median lengths of globally circulating viruses (figs. S9 and S10). We performed statistical analyses to determine the likelihood that the conserved sets of Env-specific indels that we observed in different individuals could occur

by chance and that likelihood was estimated to be vanishingly small (see “Extended Discussion” in the supplementary materials).

NAbs select for mutations in Env CH505

To examine whether NAb-mediated selection was a primary driving force in the Env-specific evolutionary patterns that we observed, early strain-specific NAb responses and later bNAb responses were mapped using site-directed mutagenesis to introduce observed mutations into neutralization-sensitive autologous and heterologous Envs. We then tested these mutant Envs, comparing against their wild-type counterparts, for sensitivity to polyclonal plasma and mAbs isolated from the infected RMs or human subjects. Variable sites in the CH505 Env (Fig. 2, A and B) were interrogated alone or in combination for their effects on Env sensitivity to autologous antibodies. Aside from variable residues in the leader sequence of gp160 that generally represent CTL escape mutations (37, 43), CTL epitope reversions to global consensus at or near residue 417 (4), and mutations at residues 300, 620, and 640 that occurred inconsistently and late in the course of infection, most of the variable residues were found to represent escape mutations from autologous NAb (fig. S11A). These included residues 234 and 334, where mutations restored PNGs that filled T/F glycan holes (fig. S3), loop D residues 279 and 281 involved in CD4 binding, CD4 contact residues in V5 (460/ΔV5), and residue 130. The temporal appearance of these NAb coincided with the appearance of phenotypically demonstrable NAb escape mutations in Env (Fig. 2, A and B). These results were corroborated by neutralization patterns of V3-targeted mAbs DH647 and DH648 and CD4bs-targeted mAbs DH650. UCA (UCA, unmutated common ancestor) and DH650 (all isolated from SHIV.CH505-infected RM6072) and the human CD4bs-targeted mAbs CH235.UCA, CH235.IA3, and CH235.9 isolated from human subject CH505 (6) (fig. S11, B and C). Human subject CH505 developed two cooperative lineages of CD4bs antibodies that targeted epitopes that included loop D residues 279 to 281 and residues in V5, eventually leading to neutralization breadth by both antibody lineages (4, 6). In RM6072, a mAb lineage, called DH650, was isolated that targeted these same epitopes, but it never developed neutralization breadth, a finding for which we found a structural explanation (see below).

In addition to the strain-specific NAb responses that we identified in SHIV.CH505-infected RMs, we found in two CH505 animals (RM5695 and RM6070) neutralizing antibodies that targeted heterologous tier 2 viruses (Fig. 1 and table S2). These bNAbs were first detected at weeks 8 (RM6070) and 16 (RM5695) after infection, and their development was tem-

porally associated with the appearance of mutations in the Env V2 apex, including residues 166 or 169 (Fig. 3A). These are common contact residues of human V2 apex bNAbs (5, 8, 48). A minor fraction of sequences lost PNGs at 156 and 160. By 24 weeks after infection in RM5695 and 32 weeks after infection in RM6070, most circulating virus contained mutations at residues 166 or 169; by 36 to 48 weeks after infection, all sequences were mutant at one or the other of these positions. We corroborated this single genome sequence evidence of strong virus selection in the central cavity of the V2 apex of RM5695 by next-generation sequencing, which revealed that 99.3% of 10,000 sequences sampled between weeks 48 and 64 after infection contained mutations at residues 166 or 169. When these residues were mutated in the wild-type versions of heterologous primary virus strains T250, Q23, MT145K, 246F, or BG505 that were otherwise neutralized by RM5695 and RM6070 plasma, neutralization was abrogated (Fig. 3C and fig. S12). Neutralization of these heterologous strains was variably dependent on the glycan at N160 (fig. S13), similar to what has been reported for V2 apex bNAbs in subject CAP256SU (49). These findings indicated the presence of potent V2 apex C-strand targeted bNAbs in RM5695 and RM6070. In summary, the mapping of autologous and heterologous NAb responses in RMs infected by SHIV.CH505 indicated that most mutations in Env that could not be ascribed to CTL selection were the result of NAb selection.

CH848

We also examined Env mutations shared between SHIV.CH848-infected RMs and the HIV-1-infected CH848 human subject as potential sites targeted by NAb. The earliest Env substitution in the human subject that was also mutated in sequences from all six RMs was at position R336, which is surface-exposed on the HIV-1 trimer. The R366G substitution in RM6167 occurred at week 10 after SHIV infection when autologous NAb titers to the T/F SHIV were 1:220. NAb titers to a site-directed mutant of the T/F virus that contained the R366G substitution fell to 1:72 (fig. S14A), indicative of an early immunodominant epitope-focused NAb response. Autologous NAb titers in RM6167 increased to 1:435 by week 36, and this was accompanied by strong selection on the evolving virus quasispecies resulting in deletions in V1 and V5 (figs. S4 and S10) and amino acid substitutions at positions indicated in fig. S4. When these consensus mutations were introduced into the CH848 T/F Env and tested for neutralization sensitivity to week 10 and 36 plasma, the mutant virus showed complete escape (fig. S14A). In human subject CH848, an early strain-specific NAb response targeted many of

these same sites including V1 (7). The virus quasispecies in subject CH848 escaped by deleting ~10 amino acids in V1, which was followed by the development of the V3 glycan-focused bNAb lineage DH270 (7, 50). Notably, the same sequence of events occurred in SHIV.CH848-infected animals RM6163 and RM6167 (fig. S10). V1 was first targeted by an early autologous NAb response (fig. S14), followed by deletions in V1, which was in turn followed by the development of V3 glycan-targeted bNAbs (Fig. 1A and table S2). We mapped the epitopes of these bNAb responses to the glycan at residue N332 and the Gly-Asp-Ile-Arg (GDIR) motif at positions 324 to 327 (Fig. 4B). Consistent with this epitope mapping, we identified, in the evolving viral quasispecies of both RMs, mutations at residues 332 to 334 and GDIR residues 324 to 327 (Fig. 4A). Like the prototypic human V3 glycan bNAbs DH270, PGT121, and PGT128, the bNAbs that we identified in RMs 6163 and 6167 were strictly N332 dependent, and mutations in spatially associated surface residues V295, N301, N138, and N133 had similar effects on neutralization potency of both rhesus and human bNAbs (Fig. 4, B and C).

CAP256

In human subject CAP256, recombination between PI and SU lineage sequences (fig. S7C) precluded a gp160-wide Env analysis. We focused instead on mutations in and near the V2 C-strand, because the human subject and two of six RMs (40591 and 42056) developed V2 apex-targeted bNAbs (Fig. 1A and table S2). In both human and RMs, very similar patterns of Env V2 sequence evolution occurred (Fig. 3B). These mutations included substitutions at the canonical residues 160, 166, 169, and 171, shown to be contact residues for other prototypic human V2 apex bNAbs (5, 8, 51–53). When introduced into heterologous neutralization-sensitive Envs, mutations at 166, 169, and 171 abrogated neutralization by plasma from RMs 40591 and 42056 as it did for control human bNAbs PGT145 and VRC26.25, the latter having been isolated from subject CAP256 (49, 53) (Fig. 3C). In RMs 40591 and 42056, we observed that V2 apex-targeted antibodies were variably dependent on binding to the glycan at Env residue 160 for neutralizing activity, a pattern that was similar to antibodies from animals RM5695 and RM6070 and human subject CAP256 (49). This variable dependence on N160 for bNAb activity is further shown in fig. S13 and is discussed in the supplementary materials. Overall, the molecular and temporal patterns of Env sequence evolution reported here for SHIV-infected macaques, and previously in humans (18, 37–39, 43), highlight the utility of dynamic measurements of localized sequence variation as a highly sensitive indicator of epitope-specific adaptive immune responses.

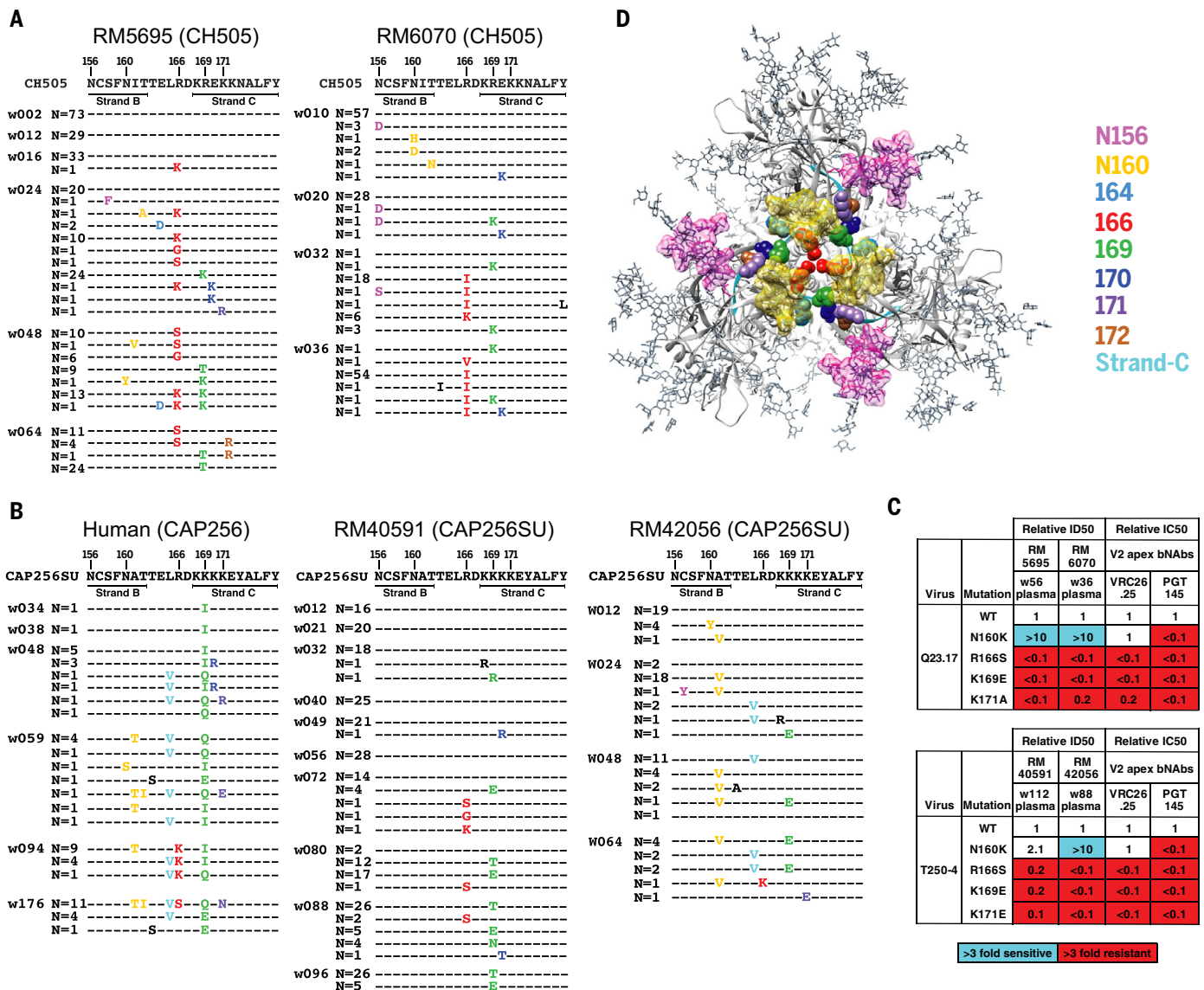


Fig. 3. Broadly neutralizing antibody responses in four rhesus macaques map to the V2 apex. (A) Single genome sequencing (N = number of sequences; w = weeks after SHIV infection) in SHIV.CH505-infected animals RM5695 and RM6070 reveals selection and fixation of mutations in and immediately proximal to strand C and additional mutations that eliminate PNG sites at 156 and 160. (B) Sequential Env sequences from human subject CAP256 and SHIV.CAP256SU-infected RMs 40591 and 42056 showed selection and fixation of mutations in and proximal to strand C,

Homologous B cell responses in humans and macaques

The observation that homologous Envs evolved in similar molecular patterns in humans and macaques could be explained by limited numbers of antigenic sites accessible for antibody binding and restricted pathways of virus escape. In addition, homologous human and rhesus germline B cell receptors could favor binding to common HIV-1 Env epitopes and follow similar patterns of Ab-Env coevolution. We explored the latter possibility by isolating and characterizing neutralizing mAbs from two RMs that were infected by SHIV.CH505.

We selected these animals for study because both exhibited favorable virus replication kinetics, comparable early NAb responses, and an overall pattern of Env evolution similar to that in the human subject CH505; nonetheless, one animal (RM5695) developed bNAbs and the other (RM6072) did not. We asked what might be the genetic and structural similarities and dissimilarities between the NAbs elicited in these animals.

CD4bs-directed antibodies

Two broadly neutralizing mAb lineages (CH235 and CH103) targeting the HIV-1 CD4bs were

previously isolated from human subject CH505, and their evolutionary pathways from germline receptors to mature antibodies were determined (2, 4, 6). In animal RM6072, serological analysis of early plasma samples suggested the presence of CD4bs-targeted Abs on the basis of selective Ab binding to CH505 T/F gp120 and resurfaced Env core but not to their isogenic Δ37II mutants, which do not bind CD4 (fig. S15A). Additional evidence of CD4bs-targeted Abs in the plasma of this animal included competitive blocking of soluble CD4 (sCD4) and CH235 and CH106 mAbs (fig. S15B). We sorted memory B cells from RM6072 from longitudinal

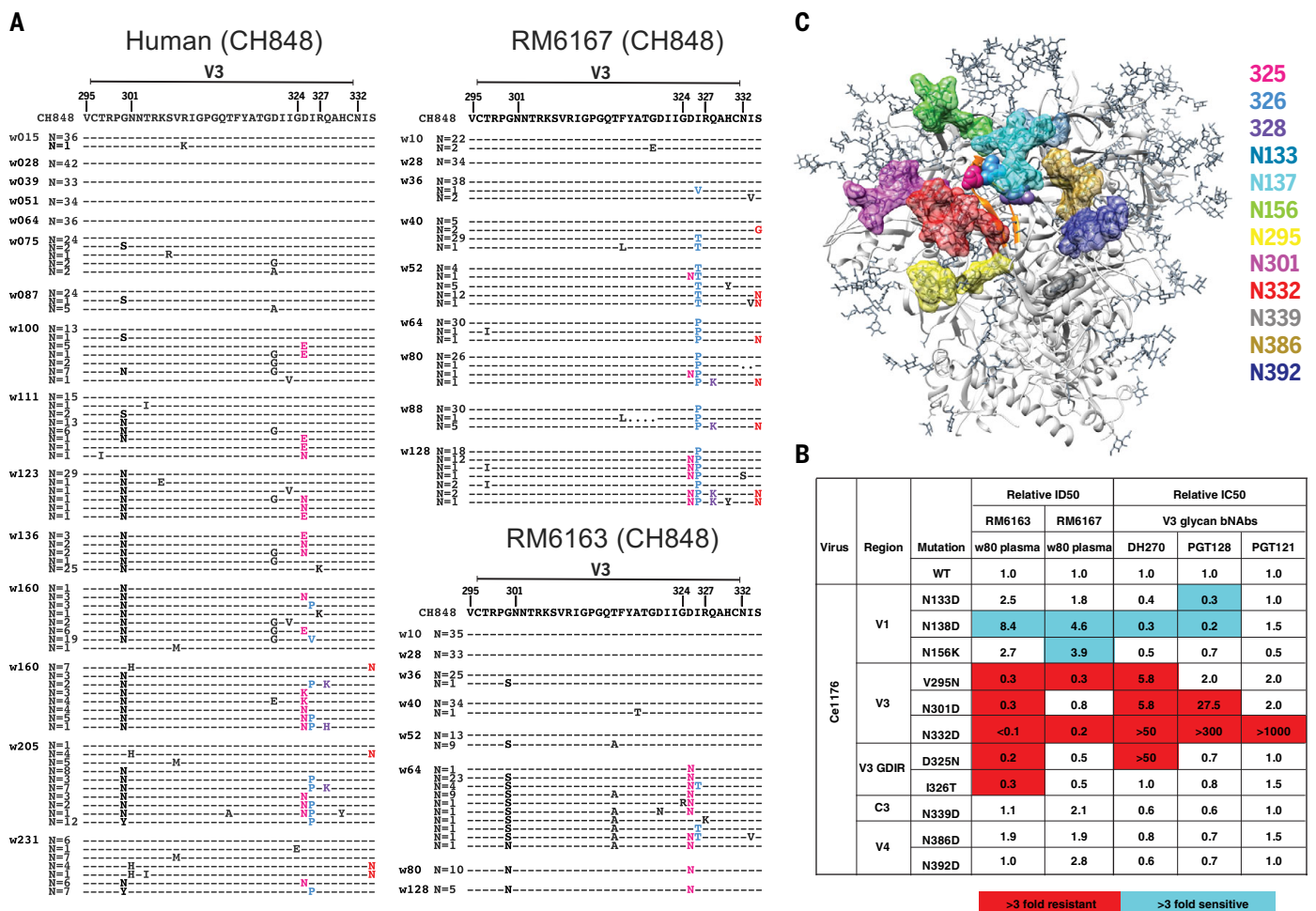


Fig. 4. Broadly neutralizing antibody responses in two rhesus macaques map to the V3 glycan high-mannose patch. (A) Sequential Env sequences from human subject CH848 and SHIV.CH848-infected RMs 6167 and 6163 showed selection and fixation of mutations in the GDIR motif. Serine-to-asparagine substitutions at position 334 shift the PNG from residue 332 to 334 in the human subject and in RM6167. **(B)** Heterologous neutralization of Ce1176 Env-pseudotyped virus by

RMs 6163 and 6167 plasma is reduced (expressed as fold-change from wild type) by mutations at N332D and V295N, consistent with human V3 glycan bNAbs. Neutralization of GDIR mutants is reduced by two- to fivefold. Elimination of a glycan at position N¹³⁸ enhances neutralization in RMs 6163 and 6167 and for some human V3 glycan bNAbs. **(C)** V3 glycan bNAB escape mutations are displayed on the 5FL structure of BG505.N332 SOSIP (side view) highlighting their close spatial proximity.

time points 20, 24, and 32 weeks after SHIV infection and selected cells that reacted with CH505 T/F gp120 but not the Δ 37II mutant. We isolated a 15-member B cell clonal lineage designated DH650 (fig. S15, C and D) that selectively bound the autologous CH505 T/F Env gp120 but not the Δ 37II mutant (fig. S15E). Some of these mAbs competed with sCD4 and CH235 and CH106 mAbs for binding CH505 T/F gp120 (fig. S15F). Mature DH650 lineage mAbs, but not the inferred germline UCA, bound CH505 T/F gp140 SOSIPv4.1 trimer (fig. S16A). Most members of the DH650 lineage neutralized a glycan-deficient mutant of CH505 Env (gly4), and two-thirds of them neutralized the wild-type CH505 T/F strain (fig. S16B). The DH650 UCA neutralized neither. None of the DH650 lineage mAbs neutralized heterologous viruses (fig. S16C and table S3).

The immunogenetic features of the DH650 lineage mAbs suggest how they recognize HIV-1

Env. The lineage comes from V(D)J recombination of the macaque V_H1-h gene (V_H, variable region of immunoglobulin heavy chain; fig. S15D), which is 91% similar to an orthologous human gene V_H1-46 used by the CD4bs bNAbs CH235 and 8ANCI31 (6, 54). DH650 antibodies share key V_H residues with CH235 (fig. S17A), which were shown previously to be contact sites with gp120 Env (6, 55). These included residue 57, which in both the CH235 UCA and DH650 UCA underwent affinity maturation to R57, which is important for CH235 bNAb activity and is shared among CD4bs bNAbs using V_H1-46 (6, 55). We found this N57R substitution in DH650 to be essential for binding to CH505 T/F Env (fig. S17B). Other DH650 V_H1-h gene residues that we found to be important for Env binding included N35, Q62, and R72 (Fig. 5 and fig. S17, C and D). A distinguishing feature of DH650 lineage antibodies was the IGVk2 light chain, which has

an exceptionally long LCDRI of 17 amino acids (fig. S17E), which we explored by structural studies.

The crystal structure of DH650 bound to the gp120 Env core of the CH505 T/F virus showed that its interactions with the gp120 CD4bs closely resembled those of the human CD4bs mAbs CH235, 8ANCI31, and VRC01 (Fig. 5, A to D, and table S4). This similarity included conserved HCDR2-mediated CD4 mimicry and coordination of Env Asp368 by Arg72. An important difference between the rhesus and human antibody lineages was in the light chains (DH650, macaque IGVk2; CH235, human IGV λ 3), in which the LCDRI of the DH650 light chain was six residues longer than its CH235 counterpart (fig. S17E). The structure showed that in the Env-Ab complex, the CH505 gp120 loop D had undergone a conformational change to accommodate the longer DH650 LCDRI. We inferred from the structure

that this shift could occur only because of the absence of a commonly found glycan at gp120 position 234 in the CH505 T/F virus. Moreover, addition of that glycan, which occurred in both the human donor and RM6072 by 30 to 36 weeks after infection, conferred resistance to DH650 (fig. S11C) and likely eliminated selective pressure in the monkey to enforce deletions in LCDR1. Thus, infection of RM6072 with SHIV.CH505 expanded a B cell clone bearing an antigen receptor encoded by the RM V_H1-h gene segment that is orthologous to the human V_H1-46 gene. This B cell lineage underwent affinity maturation, including selection for a critical R57 V_H mutation that is also found in the human CH235 bNAb lineage. It has been reported that the maturation of VRC01-class CD4bs bNAbs generally includes deletions in LCDR1 or mutations to glycine that confer flexibility (56). Evolution of the DH605 lineage in RM6072 failed to include deletions or flexibility in LCDR1 and hence neutralization breadth did not develop.

V2 apex-directed antibodies

RM5695, infected with an early SHIV.CH505 plasma virus quasispecies (see supplementary materials), developed bNAbs that, on the basis of Env escape patterns in vivo and neutralization phenotypes of site-directed Env mutants in vitro, targeted the V2 apex (Fig. 3). We used an unbiased FACS strategy to isolate 20,000 individual memory B cells from peripheral blood mononuclear cells (PBMCs) 65 weeks after SHIV infection and expanded these cells in 384-well plates. Culture supernatants were screened for neutralizing activity against two heterologous virus strains (T250-4 and Q23.17). Five wells scored positive, and paired heavy and light chain immunoglobulin genes were successfully amplified from cellular mRNA from four of them (Fig. 6A and fig. S18). All four rhesus mAbs belonged to a single lineage that we designated RHA1.V2 (rhesus HIV antibody 1 targeting a V2 epitope, with lineage members RHA1.V2.01-04). The IGVH and IGV_L genes of the four RHA1.V2.01-04 mAbs were closely related, with maximum nucleotide diversities of 5.3 and 3.9%, respectively. We used NextGen sequencing to characterize immunoglobulin transcripts expressed by naïve IgD⁺IgM⁺IgG⁻ B cells from RM5695 and used IgDiscover (57) and a recent database of RM Ig alleles (21) to identify a personalized immunoglobulin gene repertoire (table S5). From this analysis, we determined the germline origins of the mature RHA1 mAbs to include a novel IGVH4 allele, IGHV4-ABB-S*01_S8200 (fig. S18A), and IGLV1-ACN*02 (fig. S18B). Somatic hypermutation within the lineage was modest, with nucleotide divergence from germline of 7.1 to 8.5% for V_H and 6.2 to 6.6% for V_L (Fig. 6A). These values are comparable to some human V2 apex bNAbs, which typically have

lower frequencies of V_H mutations than members of other human bNAb classes. The mature rhesus bNAb heavy chains contained a two-amino acid insertion within HCDR1 (figs. S18A and S19A) and a 24-residue-long HCDR3 (IMGT numbering) that was derived from rearrangement of the V_H4-ABB-S*01_S8200, D_H3-9, and J_H2-P genes plus six nontemplated amino acids (figs. S18A and S19B). This HCDR3 was rich in aromatic and negatively charged residues, like HCDR3s of human V2 apex bNAbs (fig. S19C). Despite this long HCDR3, the ma-

ture rhesus bNAb RHA1.V2.01 was not auto- or polyreactive (fig. S20).

The HCDR3 of the RHA1 lineage antibodies was similar in length to the human V2 apex bNAb PCT64-35S (24 versus 25 amino acids, respectively), and the two broadly neutralizing mAbs contained conserved motifs within their respective HCDR3s including a negatively charged “DDY” segment (fig. S19C), which in PCT64-35S was shown to be tyrosine-sulfated and to interact with positively charged V2 apex-hole residues of Env (8, 58). All four rhesus

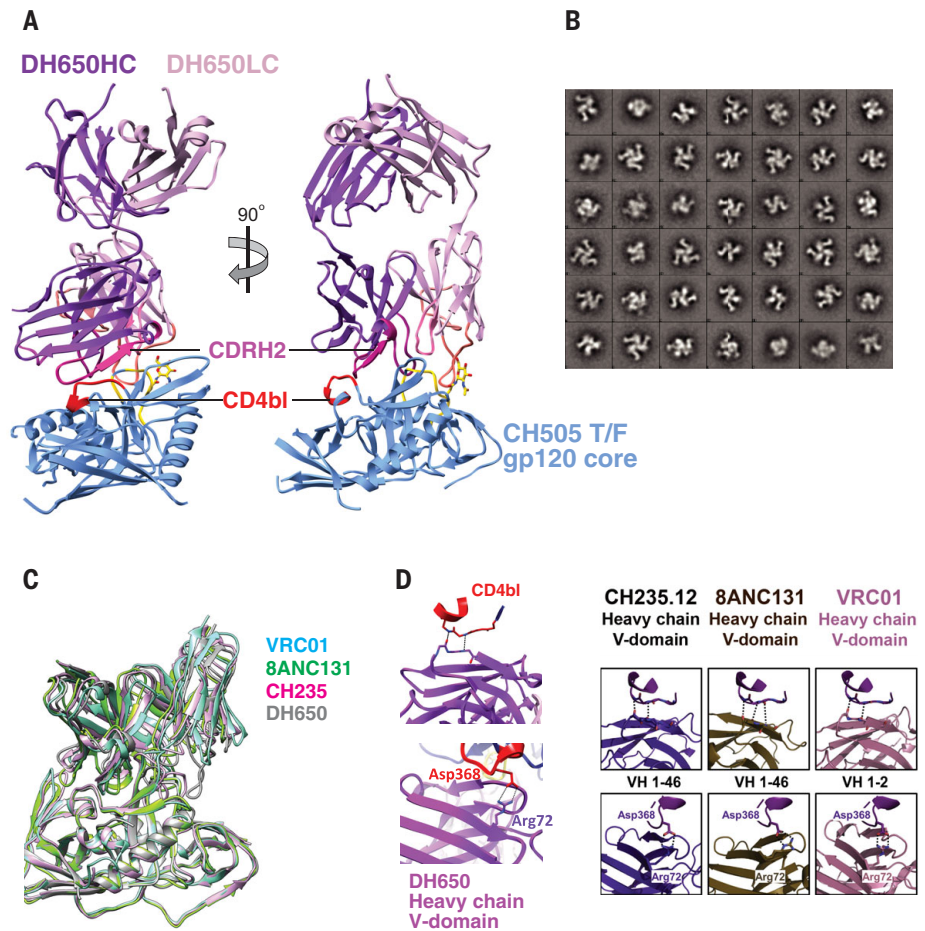


Fig. 5. Structure of Fab DH650 bound to CH505 gp120 core mimics human CD4bs antibodies.

(A) Ribbon representations of Fab DH650 heavy chain (purple) and light chain (pink) and CH505 gp120 core (blue). The heavy-chain CDRH2 is in magenta, the light-chain CDRL1 is in orange, and the CD4 binding loop (CD4bl) is in red. Loop D of gp120, which shifts from its position in other complexes to accommodate the long CDRL1 of DH650, is in yellow; the first N-acetyl glucosamine of glycan 276, which also shifts to accommodate CDRL1, is in stick representation (carbon, yellow; nitrogen, blue; oxygen, red). (B) 2D class averages after negative stain EM analysis of DH650-CH505 DS-SOSIP trimer showing three Fabs bound per trimer. (C) Superposition of Fab DH650-CH505 gp120 complex with other CD4 binding site Fab-gp120 complexes, with the essentially identical structures of gp120 as the common reference. The view corresponds to the orientation in the right-hand part of (A). Only the Fv modules of the Fabs are shown. Complex of DH650 (this study) is shown in gray, VRC01 (PDB ID 3NGB) in cyan, CH235.12 (PDB ID 5F96) in magenta, and 8ANC131 (PDB ID 4RWY) in green. DH650-bound gp120 core Cos have root mean square deviations of 0.78, 0.82, and 0.71 Å from those of the VRC01-, CH235.12-, and 8AC131-bound gp120 structures, respectively. (D) Left panel: Recognition of CD4 binding loop of CH505 T/F gp120 by variable heavy domain of DH650 (top). Coordination of Asp368 by Arg72 of DH650 (bottom). Right panel: Comparison with other CD4 binding site antibodies (6).

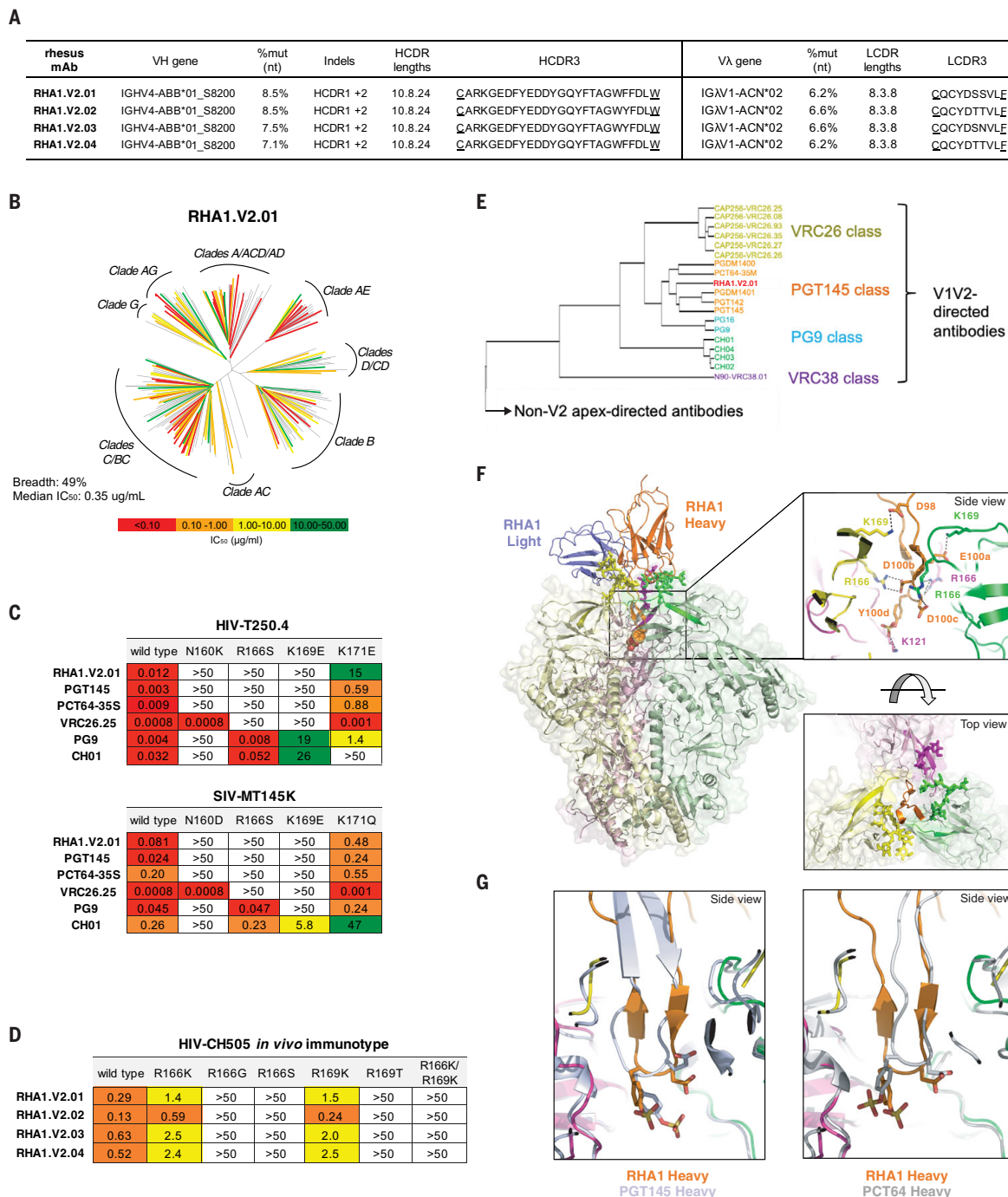


Fig. 6. Rhesus bNAb lineage RHA1 targets the V2 apex, is broadly reactive, and contains a sulfated tyrosine in HCDR3 that shows precise chemical mimicry to human bNAbs PCT64-35S and PGT145. (A) Immunogenetic characteristics of four RHA1 lineage bNAbs. A key feature is the 24–amino acid–long HCDR3 that contains an acidic EDDY core motif. **(B)** Neutralization breadth and potency of RHA1.V2.01 against a 208-strain global virus panel. The dendrogram depicts phylogenetic relatedness of the HIV-1 Envs tested. **(C)** Neutralization expressed as IC_{50} (micrograms per milliliter) of wild-type heterologous viruses and their V2 apex mutants by RHA1.V2.01 and by prototypic human V2 apex bNAbs. Like most human V2 apex bNAbs, RHA1.V2.01 is strictly dependent on N160 and positively charged residues at 166 and 169. **(D)** Neutralization of CH505 T/F (wild-type) virus and C-strand variants, or “immunotypes,” that evolved *in vivo* in RM5695. Predominant mutations at 24 weeks after SHIV infection in RM5695 were R166K or R169K; at 48 weeks, R166S, R166G, R169T, R166K, and R169K were prevalent; at 64 weeks R166S or R169T became fixed (see Fig. 3A).

Panel (D) shows progressive loss in neutralization sensitivity to RHA1 bNAbs by the evolving CH505 Envs, beginning with CH505 T/F wild type (most sensitive), CH505.R166K or R169K (intermediately sensitive), and ending with CH505.R166G, R166S, R169T, or R166K+R169K (all resistant). Results are expressed as IC_{50} (micrograms per milliliter). **(E)** Neutralization fingerprint for RHA1.V2.01 shows it to cluster within the PGT145 class. **(F)** Cryo-EM structure (side view) of RHA1.V2.01 in complex with BG505 DS-SOSIP at 4-Å resolution. Inset (top) highlights electrostatic contacts of the HCDR3 with Env protomers, including interactions of the tyrosine-sulfated 100d residue with Env K121. Inset (bottom) shows the trimer apex cavity highlighting glycans at N160 and the C-strands. **(G)** Alignment of gp120 from the complex trimer structure with RHA1.V2.01 Fab to trimer complexes with human Fabs PGT145 (PDB-5V8L) and PCT64-35S (modeled with PDB-6CA6 fit to EMD-7865) reveals alignment of tyrosine sulfated residues within the respective HCDR3 tips, which insert into the hole at the V2 apex of the Env trimer.

mAbs were tested for neutralization against the 19-member global panel of tier 2 viruses and showed similar patterns of reactivity, neutralizing 15 to 17 strains (fig. S21). One antibody (RHA1.V2.01) was tested for neutralization against a 208-member global virus panel and was found to neutralize 102 heterologous virus strains, or 49%, at a maximum concentration threshold of 50 $\mu\text{g/ml}$ (Fig. 6B and fig. S22). Neutralization of heterologous virus strains depended on Env residues N160, R/K166, and R/K169, with partial dependence on K171 (Fig. 6C and fig. S23). This precise pattern of neutralization sensitivity to N160, R/K166, and C-strand residue R/K169 and K171 mutations was shared by the human V2 apex bNAbs PCT64-35S and PGT145 but was different from that of PG9, VRC26.25, and CH01. CH505 Envs that evolved in RM5695 *in vivo* coincident with the development and maturation of RHA1 lineage antibodies showed evidence of strong selection at residues 166 and 169 (Fig. 3A). Introduction of these mutated residues into the CH505 T/F Env resulted in loss of neutralization sensitivity to RHA1 mAbs (Fig. 6D).

Bioinformatical comparisons of human and RM V2 apex bNAbs

Using a neutralization “fingerprint” analysis (59), which compares the potency of individual bNAbs against a large set of HIV-1 strains (fig. S22), we observed clustering of RHA1.V2.01 within the PGT145 class of V2 apex bNAbs that includes PCT64-35M and PGDM1400 (Fig. 6E and fig. S19, D and E). In a hierarchical clustering analysis of the neutralization profiles of RHA1.V2.01 and other prototypic human V2 apex bNAbs measured against the 208-virus panel, RHA1.V2.01 grouped most closely with PCT64-35M (fig. S24A). This finding was strongly supported statistically by the overlap of viruses that were sensitive or resistant to those antibodies [Fisher’s exact test $P = 2 \times 10^{-16}$; odds ratio = 13.14; accuracy ratio = 0.78 (all concordant = 1; none = 0)] (fig. S24B) and by correlation of median inhibitory concentration (IC_{50}) titers of RHA1.V2.01 and PCT64-35M (coefficient of determination $R^2 = 0.4467$; $P = 1.4 \times 10^{-10}$) compared with other V2 apex bNAbs (fig. S24C). We next examined neutralization profiles across different HIV-1 group M subtypes (fig. S25). We found that RHA1.V2.01 was more subtype-independent than any of the human V2 apex bNAbs but was otherwise most similar to PCT64-35M and CAP256.VRC26. Finally, we performed a neutralization signature analysis using GenSig (www.hiv.lanl.gov/content/sequence/GENETICSSIGNATURES/gs.html) (fig. S26). Neutralization “signatures” identify individual Env residues that contribute directly or indirectly to antibody binding, including those potentially involved in selecting for affinity maturation (60). The signa-

ture analysis was performed using Fisher’s test with a binary IC_{50} threshold greater or less than 50 $\mu\text{g/ml}$ and a Wilcoxon test that measures the difference in IC_{50} distributions with and without a given amino acid residue. High-confidence signature sites were defined as those meeting at least two of three criteria: (i) contact sites; (ii) at least one phylogenetically corrected signature at the site; or (iii) at least one signature at the site that had a false discovery rate $q < 0.1$. For the rhesus mAb RHA1.V2.01, statistically robust signatures were identified at residues 130, 160, 166, 167, and 169. Among all of the V2 apex bNAbs analyzed, only PCT64-35M shared all five of these signature sites.

Structure of V2 apex bNAb RHA1.V2.01

The structure of mAb RHA1.V2.01 in complex with the BG505 DS-SOSIP Env trimer, determined by cryo-electron microscopy (cryo-EM) at 3.9-Å resolution, showed notable similarity to PGT145 and PCT64-35S (Fig. 6, F and G, and table S6). These antibodies bind Env with a 1:1 stoichiometry near the trimer threefold axis and are surrounded by the three N160 glycans. Their respective HCDR3s adopt a needle-like antiparallel β -hairpin conformation that extends from the combining surface of the Fab and inserts into a cationic hole at the trimer apex. The N-terminal ends of each of the three C-strands abut the apex hole and are oriented perpendicular to the inserting HCDR3. Like PCT64-35S and PGT145, the acidic EDDY motif of RHA1.V2.01 was tyrosine-sulfated and made key contacts with Env residues 121, 166, and 169. (Fig. 6F, boxed insert). When the Env-bound structures of RHA1.V2.01, PCT64-35S, and PGT145 were overlaid, the respective EDDY motifs aligned at the tips of their respective HCDR3 loops around the β -hairpin turn (Fig. 6G). Otherwise, the overall Fab orientations differed, indicating the HCDR3 tip structural mimicry to be the main source of the neutralization similarity among these antibodies. The HCDR1 of RHA1.V2.01, which contained a nontemplated two-amino acid insertion in addition to other strongly selected mutations, was sandwiched between the Env N160 glycans of two protomers and proximal to the C-strand of one, with buried surface area of 52 and 49 Å², respectively, for the two glycans and a key electrostatic interaction between D29 and K171 (Fig. 6F and figs. S19A and S27F). Thus, the V2 apex bNAb lineage in RM5695 exhibits genetic, chemical, and structural solutions to epitope recognition that are shared with human V2 apex targeted bNAbs, especially PCT64-35S and PGT145.

Discussion

A principal finding of this study is that SHIVs bearing primary T/F HIV-1 Envs elicit strain-specific and heterologous NAb in RMs that

can replicate to a considerable degree responses to HIV-1 in humans. This mimicry includes the frequency, kinetics, titers, immunogenetics, structures, and target epitopes of elicited antibodies; structural and chemical features of epitope recognition; and coevolutionary pathways of antibody maturation and Env escape. All are key features to be considered in vaccine design. Our findings add substantially to earlier reports of sporadic neutralization of heterologous tier 2 viruses elicited in RMs by SHIVs bearing lab-adapted or animal-passaged HIV-1 Envs (61–64) or Env immunogens (65–72). The current results, together with a recent report by Wang and colleagues (73), show how closely neutralizing antibody responses in RMs can mirror responses in humans and indicate the extent to which protective responses elicited by reverse engineered or lineage-based vaccines in RMs might be expected to predict human responses to candidate vaccines (10, 11, 74, 75).

While bNAbs from animal RM5695 were exceptional, the breadth and potency of bNAbs from the other six animals were more in keeping with a large cross section of chronically infected humans who were studied for neutralization breadth generally after many years of infection (28, 33, 34). In those studies, “elite neutralizers”—those with the most broadly reactive antibodies and from whom many of the best bNAb mAbs have been isolated—actually represented a very small fraction (<5%) of infected individuals. What is most notable about our study is not the overall breadth and potency of rhesus bNAb responses but the fact that we observed bNAbs arising in 7 of 22 prospectively studied animals after less than 1 or 2 years of SHIV infection and that the epitope specificities of these antibodies could be mapped to canonical HIV-1 bNAb sites in six. These findings suggest that the rhesus macaque is a favorable model for HIV-1 vaccine studies where the key variables of priming, boosting, affinity maturation, and antibody durability can be explored rapidly and iteratively.

An unexpected observation was the extent to which Env evolution in macaques recapitulated evolution of homologous Envs in human infections. Similarities included site-specific and amino acid-specific mutations and identities or near-identities of indels. These similarities likely resulted from: (i) the highly evolved and functionally constrained nature of primary T/F Env trimers, (ii) limited sites of antibody accessibility and variable fitness costs of escape mutations, and (iii) homologous germline B cell responses in different animals and humans to conserved Env epitopes. Equally surprising were the genetic and structural similarities between rhesus and human antibodies that targeted CD4bs or V2 apex epitopes and their conserved mechanisms of epitope recognition. This included the HCDR2-mediated CD4 mimicry of the

rhesus antibody DH650 and the tyrosine-sulfated, 24-residue-long HCDR3 of the rhesus antibody RHA1.V2.01, which bound N160 glycans and positively charged Env residues at positions 121, 166, 169, and 171. Together, the conserved patterns of Env-specific sequence variation and the homologous and orthologous B cell responses in humans and RMs represent notable examples of convergent evolution (14) that may aid in the design and testing of novel HIV-1 vaccines.

Our findings suggest that HIV-1 Envs are not equal in their propensity for eliciting epitope-specific bNAb responses. For example, we found that CAP256SU Env, which elicited V2 apex bNAbs in human subject CAP256 (3, 5, 22), induced bNAbs of the same specificity in two of six SHIV-infected RMs. CH848 Env, which elicited V3 glycan targeted bNAbs in a human subject (7), did the same in 2 of 6 SHIV infected RMs. And CH505 Env, which elicited CD4bs targeted bNAbs in a human subject (2, 4, 6), induced homologous strain-specific CD4bs targeted NAb in RM6072. CH505 Env also elicited V2 apex targeted NAb with variable breadth in vaccinated CH03 heavy chain Ig knock-in mice and an immunized RM (69). In the present study, it did so as well in 2 of 10 SHIV infected RMs. In still other SHIV infected RMs, we have identified fusion peptide targeted bNAbs and broadly reactive and potent CD4bs bNAbs. These findings highlight the potential for RMs to develop antibody responses targeting an array of different canonical bNAb epitope clusters and suggest a tendency for certain Envs to preferentially elicit bNAb responses targeting particular epitopes.

SHIV replication in RMs is the only model system other than naturally infected humans where the immunogen (Env) coevolves with antibodies. The high mutability and dynamic replication of HIV-1 and SHIV result in a constantly evolving virus quasispecies (9, 18, 38, 39, 42, 43), which means that Envs with binding affinities sufficient to drive bNAb lineage affinity maturation are constantly being generated. The SHIV-infected macaque can therefore be particularly informative for vaccine design by enabling the identification and then rapid testing of Env intermediates that guide the evolution of germline bNAb precursor B cells through stages of affinity maturation to acquire breadth and potency. In the CAP256 (5) and PC64 (8) infected human subjects, viral sequences showed very similar patterns of Env evolution at residues 166 and 169, which in turn were similar to the pattern in the SHIV. CH505-infected RM5695. Deep sequencing of RM5695 plasma vRNA covering the V1V2 region revealed selection focused primarily on residues 166 and 169 with mutations at these two sites rapidly and completely replacing the infecting virus strain. The infecting SHIV. CH505 virus had an Arg at these two positions,

which evolved progressively to R166K or R169K and then to R166G, R166S, or R166T (Fig. 3). The earliest mutants, R166K and R169K, were approximately fivefold more resistant to the mature rhesus bNAb mAbs than the infecting virus, whereas the subsequent R166G, R166S, and R166T mutants were >100-fold more resistant (Fig. 6D). Thus, sequential Envs that varied at residues 166 and 169 in animal RM5695 showed progressive phenotypic escape from V2 apex bNAb antibodies, closely resembling the viral Env-bNAb coevolution observed in humans CAP256 and PC64. Cryo-EM analysis of the RHA1.V2.01 mAb provided a structural explanation for this loss of antibody recognition by showing that Env residues 166 and 169 were primary electrostatic contacts with the antibody. Mutations in these two residues in the V2 apex appear to be largely or solely responsible for driving affinity maturation of diverse antibody lineages to breadth in multiple rhesus animals and humans within a relatively short time (<1 year), suggesting that Env intermediates or “immunotypes” (5) required for V2 apex bNAb elicitation may be few and simple. This hypothesis has important implications for V2 apex-targeted HIV-1 vaccine design, which can be tested rapidly in Ig knock-in mice and outbred macaques using immunogens designed from V2 apex variants of CH505 and other primary Envs. The goal of such research would be to learn the rules governing consistent bNAb induction in RMs and then translate these findings to human studies using SOSIP, mRNA, or other non-SHIV-based vaccine platforms.

V3 high-mannose patch glycopeptides are also commonly targeted by bNAbs in HIV-1-infected humans (33) and are of high interest for HIV-1 vaccine development (50, 76, 77). Site-directed mutagenesis coupled with antibody neutralization showed that polyclonal bNAb responses in SHIV.CH848-infected RMs 6167 and 6163 targeted canonical N332 and ³²⁴GDIR³²⁷ motifs, similar to human V3 glycan bNAbs (78, 79). Deletions in V1 of SHIV.CH848 sequences preceded the development of V3 glycan bNAbs in both monkeys and human subject CH848. Long, glycosylated (N133 and N138) V1 segments obstruct access of V3 glycan bNAbs (7, 80), and germline-targeted Env immunogens with shortened V1 segments depleted of glycans enhance Ab access to V3 high-mannose patch epitopes (50, 76). Because Env-Ab coevolution leading to V3 glycan bNAbs generally requires more extensive somatic hypermutation compared with V2 apex bNAbs (10, 11), a rhesus model in which vaccinations with germline-targeted Envs (50, 76, 77) is followed by infection with SHIVs whose Envs are similarly targeted, offers a novel strategy for identifying the “finishing” or “polishing” immunogens necessary for bNAb affinity maturation and an outbred primate model system to test them.

It is generally believed that the development of an effective neutralizing antibody-based HIV-1 vaccine will require consistent activation of multiple germline precursor B cells that express immunoglobulin receptors specific for one or more of the canonical bNAb epitope clusters, followed by efficient antigen-driven selection for antibody affinity maturation (10, 11, 50, 74–77, 81). The present study demonstrates that the SHIV-infected rhesus model can inform both of these critical steps in bNAb elicitation. The fact that only a minority of SHIV infected animals in the current study developed bNAbs is a faithful reflection of the natural prevalence of bNAb responses in HIV-1-infected humans (28, 33, 34, 82) and further argues for the relevance of the rhesus model. A clear limitation of our study is that SHIV infection is not a viable vaccine strategy for humans nor is CD8 depletion, which was employed to increase peak and set point virus loads. Nonetheless, it should be possible to combine established immunization platforms such as Env trimers, outer domain scaffolds, virus-like particles, or DNA and RNA expression followed by SHIV infection to identify optimized priming and boosting immunogens that elicit broad neutralization in macaques as a molecular guide for HIV-1 vaccine design in humans.

Materials and methods

Nonhuman primates and SHIV inocula

Indian RMs were housed at Bioqual, Inc., Rockville, MD, according to guidelines of the Association for Assessment and Accreditation of Laboratory Animal Care standards. Experiments were approved by the University of Pennsylvania and Bioqual Institutional Animal Care and Use Committees. RMs were sedated for blood draws or excisional biopsies of lymph nodes, anti-CD8 mAb infusions, and SHIV inoculations. A subset of animals received an intravenous infusion of either 25 to 50 mg/kg of anti-CD8 α mAb (MT807R1) or anti-CD8 β mAb (CD8beta255R1) 1 week before or at the time of SHIV inoculation. The intent of administering anti-CD8 mAbs was to transiently reduce CD8⁺ cells, thereby allowing for higher peak and set point viral loads. This was done in only a subset of animals because it was not known a priori whether this might accelerate disease progression to an extent that would preclude long-term follow-up of animals for bNAb induction. In humans, higher plasma virus loads and lower CD4⁺ T cell counts are correlated with the development of bNAbs (33, 34). SHIV infections were done intravenously. All animals in this study, with the exception of RM5695, were inoculated with molecularly cloned virus [50 or 500 ng p27Ag in Dulbecco's modified Eagle's medium (DMEM) or RPMI 1640 with 10% heat-inactivated fetal bovine serum (FBS)] containing the preferred

Env375 variant or a mixture of Env375 Env variants. Animals RM6069, 6070, 6072, 6163, and 6167 were repurposed from a previous study of SHIV replication dynamics and immunopathogenesis (9). Animal RM5695 was repurposed from a previous study of HIV-1 CH505 Env gp120 protein immunization (23). This animal was infected with 0.2 ml of SHIV-positive plasma from monkeys RM6069 (weeks 10 and 20), RM6070 (weeks 10 and 20), and RM6072 (weeks 4, 10, and 20), for a total plasma inoculum of 1.4 ml. The rationale for this experiment was to increase early viral diversity and potentially include antigen-antibody immune complexes in the inoculum. The genetic composition of this plasma virus inoculum, and the particular viral genomes that were successfully transmitted to RM5695, can be seen in the *Highlighter* and *LASSIE* panels in Fig. 2, A and B, and the sequences can be accessed from GenBank (accession # MT484881-MT484977).

Processing and storage of clinical specimens

All blood samples were collected in sterile vacutainers containing acid citrate dextrose formula A (ACD-A) anticoagulant. ACD-A anticoagulated blood (40 ml) was combined in a sterile 50-ml polypropylene conical tube, centrifuged at 2100 revolutions per minute (rpm) (1000g) for 10 min at 20°C, and the plasma collected in a fresh 50-ml conical tube without disturbing the buffy coat white blood cell (WBC) layer and large red cell pellet. The plasma was centrifuged again at 2500 rpm (~1500g) for 15 min at 20°C to remove all platelets and cells. Plasma was collected and aliquoted into 1-ml cryovials and stored at -80°C. The red blood cell (RBC)/WBC pellet was resuspended in an equal volume of Hanks balanced salt solution (HBSS) without Ca⁺⁺ or Mg⁺⁺ and containing 2 mM EDTA and then divided into four 50-ml conical tubes. Additional HBSS-EDTA (2 mM) buffer was added to bring the volume of the RBC/WBC mixture to 30 ml in each tube. The cell suspension was then carefully underlayered with 14 ml 96% Ficoll-Paque and centrifuged at 1800 rpm (725g) for 20 min at 20°C in a swinging bucket tabletop centrifuge with slow acceleration and braking so as not to disrupt the Ficoll-cell interface. Mononuclear cells at the Ficoll interface were collected and transferred to a new 50-ml centrifuge tube containing HBSS-EDTA (without Ca⁺⁺ or Mg⁺⁺) and centrifuged at 1000 rpm (~200g) for 15 min at 20°C. This pellets PBMCs and leaves most of the platelets in the supernatant. The supernatant was removed, and the cell pellet was resuspended in 40 ml HBSS (with Mg⁺⁺ and Ca⁺⁺ and without EDTA) + 1% FBS. To remove additional contaminating platelets, the cell suspension was centrifuged again at 1000 rpm (~200g) for 15 min at 20°C and the supernatant discarded. The cell pellet was tap-resuspended in the residual 0.1 to 0.3 ml of media and then brought to a volume of 10 ml

HBSS (with Mg⁺⁺ and Ca⁺⁺) + 1% FBS. Cells were counted and viability assessed by trypan blue exclusion. Cells were centrifuged again at 1200 rpm (300g) for 10 min at 20°C, the supernatant discarded, and the cells resuspended at a concentration of 5 to 10 × 10⁶ cells/ml in CryoStor cell cryopreservation media (Sigma cat. no. C2999) and aliquoted into 1-ml cryovials (CryoClear cryovials; Globe Scientific Inc., cat. no. 3010). Cells were stored in a Corning CoolCell LX cell freezing container at -80°C overnight and then transferred to vapor-phase liquid N₂ for long-term storage. Mononuclear cells collected from lymph nodes (LN) and spleen were processed in a similar manner to blood mononuclear cells. LN and spleen were excised and placed immediately into RPMI1640 medium on wet ice. LNs were diced with a sterile scalpel, and spleen was homogenized and the material passed through a sterile mesh grid. Cells were collected from the pass-through and subjected to Ficoll density gradient purification as described above.

SHIV construction and characterization

The experimental design for constructing SHIVs bearing primary or T/F Envs with allelic variation at gp120 residue 375 was previously described, including SHIV.CH505 and SHIV.CH848 (9). For the construction of SHIV.CAP256SU, we synthesized (GenScript) sequence KF996583.1 from GenBank (GenBank: KF996583.1) and cloned it into the pCRXL-TOPO-SIVmac766 backbone (9) by recombinant polymerase chain reaction (PCR). The QuikChange II XL Site-Directed Mutagenesis kit (Agilent Technologies) was used to create allelic variants (M, Y, F, W, or H) of the wild-type Env375S codon. Wild-type and mutant plasmids were transformed into MAX Efficiency Stbl2 Competent Cells (Invitrogen) for maxi-DNA preparations. Each 10-kb viral genome was sequenced in its entirety to authenticate its identity. Infectious SHIV stocks were generated in 293T cells as previously described (9). On day 0, five million 293T cells were plated in 100-mm tissue culture dishes in 10 ml of complete MEM growth media with 10% FBS. On day 1, 6 µg of SHIV plasmid DNA was combined with 18 µl of FuGENE 6 (Promega) in 500 µl of DMEM was added dropwise to tissue culture dishes. Media containing virus was harvested on day 3 and aliquoted for storage at -80°C. Virus concentration was estimated by p27 antigen (p27Ag) ELISA (Zeptomatrix) and infectious particle concentration was determined by entry into TZM-bl cells in the presence of DEAE-Dextran, as previously described (18). Typically, 293T-derived SHIV stocks contained >1000 ng/ml p27Ag and >1,000,000 IU/ml on TZM-bl cells. The replication kinetics of each of the SHIV.CAP256SU Env375 variants in primary, activated human and rhesus CD4 T cells were determined as previously

described (9). 293T supernatants containing 300 ng p27Ag of each variant were added to 2 × 10⁶ purified human or rhesus CD4 T cells in complete RPMI growth medium [RPMI1640 with 15% FBS (Hyclone), 100 U/ml penicillin-streptomycin (Gibco), 30 U/ml IL-2 (aldesleukin, Prometheus Laboratories), and 30 µg/ml DEAE-Dextran]. As 300 ng p27Ag is equal to ~3 × 10⁹ virions, ~3 × 10⁵ IU on TZM cells, or ~3 × 10⁴ IU on primary CD4 T cells, the estimated MOI of this titration was estimated to be about 0.01. The cell and virus mixtures were incubated for 2 hours under constant rotation at 37°C to facilitate infection, washed three times with RPMI1640, and resuspended in complete RPMI1640 medium lacking DEAE-Dextran. Cells were plated into 24-well plates at 2 million cells in 1 ml and cultured for 11 days, with sampling of 0.2 ml supernatant and media replacement every 2 to 3 days for 11 days. Supernatants were assayed for p27Ag concentration by ELISA (Zeptomatrix).

Plasma vRNA quantification

Plasma viral load measurements were performed by the NIH/NIAID-sponsored Non-human Primate Virology Core Laboratory at the Duke Human Vaccine Institute. This core facility is CLIA certified and operates a highly standardized, quality-controlled Applied Biosystems Real-Time SIV and HIV vRNA PCR assays. QIASymphony SP and QIAGEN automated platforms (QIAGEN) are used for high-throughput sample processing and PCR setup. Viral RNA is extracted and purified from plasma, annealed to a target specific primer and reverse transcribed into cDNA. The cDNA is treated with RNase and added to a custom real-time PCR master mix containing target specific primers and a fluorescently labeled hydrolysis probe. Thermal cycling is performed on a QuantStudio3 (ThermoFisher Scientific) real-time quantitative PCR (qPCR) instrument. Viral RNA copies (cp) per reaction is interpolated using quantification cycle data. Raw data are quality-controlled, positive and negative controls are checked, and the mean viral RNA cp per milliliter is calculated. Over the course of this study, the sensitivity limits for accurate vRNA quantification using 0.5 ml of NHP plasma improved from 250 RNA cp/ml to 62 RNA cp/ml. We chose a conservative threshold of 100 RNA cp/ml for a limit of detection and 250 RNA cp/ml for the limit of quantification.

Viral sequencing, pixel plots, and LASSIE analysis

Single genome sequencing of SHIV 3' half genomes was performed as previously described (1, 9). Geneious R7 was used for alignments and sequence analysis and sequences were visualized using the LANL Highlighter and Pixel tools (www.hiv.lanl.gov/content/sequence/pixel/pixel.html and www.hiv.lanl.gov/content/sequence/HIV/HIVTools.html; 44). The specific

implementation of this software for this project is described in the figure legends.

IgG isolation from plasma

Total polyclonal IgG was isolated from rhesus plasma using the Protein A/Protein G GraviTrap kit (GE Healthcare). Plasma was heat-inactivated (1 hour at 56°C), clarified by centrifugation at 21,000g for 4 min, and applied to the Protein A/G column. The sample was washed and eluted per the manufacturer's instructions and then buffer-exchanged with phosphate-buffered saline (PBS). The concentration of purified IgG sample was quantified using the Pierce BCA Protein Assay Kit (ThermoFisher).

Neutralizing antibody assay

Assays for neutralizing antibodies were performed using TZM-bl indicator cells, as previously described (9, 18). This assay is essentially identical to that used by Montefiori, Seaman, and colleagues (83) (www.hiv.lanl.gov/content/nab-reference-strains/html/home.htm), the only difference being that in our assay we plate virus and test plasma onto adherent TZM-bl cells and hold the concentration of test plasma constant (5% v/v) constant across all wells, which contain 10% heat-inactivated fetal bovine serum in the complete RPMI1640 culture medium. Target viruses express HIV-1 Envs whose complete designations and subtype classifications are included in fig. S22 and table S3 and reported elsewhere (26, 27, 84). In Fig. 1A, we calculated neutralization breadth ($ID_{50} \leq 0.05$) across all time points for each animal from titers displayed in table S2 and plotted in Fig. 1A. We calculated the maximum geometric mean titer (GMT) of neutralization at any one time point from values with $ID_{50} \leq 0.05$, as displayed in table S2 and plotted in Fig. 1A.

Binding antibody assays

HIV-1 Env binding by recombinant mAbs and plasma or sera were tested in ELISA, as previously described (50, 85). In brief, recombinant Envs were coated directly to Nunc-adsorb (ThermoFisher) plates overnight at 4°C or captured using AbC- mAb (AVIDITY, Colorado, USA) that was directly coated to Nunc-adsorb plates overnight at 4°C. Antibody binding was detected with goat anti-human or goat anti-rhesus HRP-labeled anti-IgG Fc antibodies (Jackson ImmunoResearch Laboratories), and HRP detection was subsequently quantified with 3,3',5,5'-tetramethylbenzidine (TMB). Competitive ELISA to assess cross-blocking of recombinant mAbs or plasma antibodies were previously described (7, 86). We biotinylated the antibodies using BIOTIN-X-NHS (Cayman Chemicals, CAT# 13316). Competitive inhibition of biotinylated mAbs was measured as a percent of binding in the presence of a competing nonbiotinylated mAb relative to binding in the absence of this competing mAb. MABs

were also tested for binding HIV-1 Envs using Biolayer interferometry (BLI) as described (87). Here, antibody binding was measured using mAb-captured sensors that were placed into solutions of CH505 gp120 or SOSIP trimers at 50 µg/ml for 1000 s. MABs were captured using anti-human IgG Fc sensors, and nonspecific or background binding was subtracted using binding levels by anti-influenza HA mAb (CH65).

Rhesus B cell staining and sorting of strain-specific mAbs

CH505 gp120 T/F CD4bs-specific antibodies were isolated from memory B cells in PBMCs, lymph node, or bone marrow collected at weeks 20, 24, 32, and 52 using two approaches: direct single-cell sorting into PCR plates (weeks 20, 32, and 52) (23, 88) and memory B cell cultures (week 24) (89, 90). For direct sorting, we performed single-cell isolation of memory B cells decorated with AlexaFluor 647 (AF647) or Brilliant Violet 421 (BV421)-tagged HIV-1 CH505 TF gp120 using a BD FACSAria or a BD FACSAria II (BD Biosciences, San Jose, CA), as previously described (23). The flow cytometry data were analyzed using FlowJo (Treestar, Ashland, OR) (88, 91, 92). For our sort strategy, we isolated antigen-specific IgD-negative, CD27-All memory B cells that bound BV421-tagged CH505 T/F gp120 but not AF647-tagged CH505 T/F gp120 Δ371 mutant protein; antibodies isolated from these B cells were referred to as CH505 differential binders or CD4BS antibodies (23). For memory B cell cultures, from 8 million PBMCs, we sorted 30,792 CH505 T/F gp120-specific B cells, defined as CD3-negative, CD14-negative, CD16-negative, IgD-negative, CD27-All, CD20-positive, AF647-tagged CH505 T/F gp120-positive and BV421-tagged CH505 T/F gp120-positive. As previously described (90), cells were flow sorted in bulk into wells containing 5000 MS40L feeder cells, RPMI-1640 supplemented with 15% FBS, 1 mM sodium pyruvate, 1% non-essential amino acids, 25 mM HEPES buffer, 2.5 µg/ml ODN2006 (Invivogen, TLR1-2006-5), 5 µM CHK2-inhibitor (Calbiochem, 220486), 100 ng/ml recombinant human interleukin (IL)-21 (Peprotech, cat. no. 2001-21), 10 ng/ml recombinant Human BAFF (Peprotech, cat. no. 310-13), 200 U/ml IL-2 (from the myeloma IL-2 producing cell line IL-2t6, provided by A. Lanzavecchia, IRB, Bellinzona, Switzerland), and 100 µl supernatant of the *Herpesvirus papio* (HVP)-infected Baboon cell line S594 (NHP Reagent Resource). The concentration of each supplement was previously determined to achieve optimal in vitro stimulation. After overnight incubation at 37 °C in 5% CO₂, memory B cells were transferred at limiting dilution into 96-well round-bottom tissue culture plates containing 5000 MS40L feeder cells. Culture medium was refreshed 7 days after plating and harvested 2 weeks after plating to test for binding to CH505 T/F gp120, CH505 T/F gp120 Δ371, RSC3 (93), and RSC3 Δ371 P363N,

as well as for neutralization of pseudotyped the CH505 T/F HIV-1 strain in the TZM-bl-based neutralization assay using a single dilution of supernatant (89, 94). CD4bs DH650 lineage autologous tier 2 NABs were isolated from CH505 differential-binding memory B cells in PBMCs from week 20, 24, and 32 after SHIV CH505 infection of RM6072. In capturing maximum numbers of B cells bearing candidate CD4bs antibodies, we used a less stringent gating strategy for capturing CH505 T/F gp120 (+) and CH505 T/F gp120 Δ371 (-) B cells. In so doing, we also captured non-CD4 binding site autologous tier 2 NABs, including DH647 and DH648 that were isolated from memory B cells in PBMCs at week 20 after SHIV infection of RM6072.

Rhesus B cell staining, culture, and microneutralization screening for V2 apex bNABs

Cryopreserved PBMCs from RM5695 at week 65 after SHIV infection were thawed and stained with LIVE/DEAD Fixable Aqua Dead Cell Stain (Life Technologies), as previously described (95, 96). Cells were washed and stained with an antibody cocktail of CD3 (clone SP34-2, BD Biosciences), CD4 (clone OKT4, BioLegend), CD8 (clone RPA-T8, BioLegend), CD14 (clone M5E2, BioLegend), CD20 (clone 2H7, BioLegend), IgG (clone G18-145, BD Biosciences), IgD (polyclonal, Dako), and IgM (clone G20-127, BD Biosciences) at room temperature in the dark for 20 min. The stained cells were washed three times with PBS, resuspended in 1 ml of PBS and passed through a 70-µm cell mesh (BD Biosciences). Total memory B cells (CD3-CD4-CD8-CD14-CD20+IgD-IgM-IgG+) were sorted with a modified three-laser FACSAria cell sorter using the FACSDiva software (BD Biosciences) and flow cytometric data were subsequently analyzed using FlowJo (v9.7.5). B cells were sorted at 1 cell per well of a 384-well plate containing B cell culture media following a human B cell culture protocol (97) that was optimized for the expansion of rhesus B cells. Briefly, sorted B cells were expanded for 14 days in B cell culture medium consisting of Iscove's modified Dulbecco's medium (IMDM) with GlutaMAX supplemented with 10% heat-inactivated FBS, 1X MycoZap Plus-PR, 100 U/ml IL-2, 0.05 µg/ml IL-4, 0.05 µg/ml IL-21, 0.05 µg/ml BAFF, 2 µg/ml CpG ODN2006, and 3T3-msCD40L feeder cells at a density of 5000 cells per well. Supernatants from ~14,000 individual wells were evaluated for neutralization of HIV-1 Q23.17 and T250-4 Env-pseudotyped viruses using the high throughput NVITAL automated microneutralization assay, as previously described (98). Wells were selected for RT-PCR on the basis of 50% reduction in infectivity of at least one virus. Out of nearly 14,000 wells tested, five met these neutralization criteria. Paired heavy and light Ig chains were successfully amplified from four of these wells. These amplicons were sequenced, cloned, and expressed as IgG1 (RHA1V2.01-04),

and all four mAbs exhibited broad and potent neutralization.

Rhesus B cell cloning and expression

Heavy (IGHV) and light (IGKV, IGLV) chain genes were isolated via single cell PCR approaches (88, 99), and the gene sequences were computationally analyzed using rhesus Cloanlyst program (100–102). Antibody immunogenetics were reported as gene families and segments, mutation frequencies, and CDR3 lengths using the rhesus Cloanlyst database of reference genes (21). Using the rhesus cloanlyst program, we identified B cell clonal lineages for antibodies with the same inferred IGHV VDJ rearrangement and CDR3 length, and paired with the same light chain (Ig VJ segments). For DH650 lineage, the UCA and intermediate (IA) genes were inferred computationally using the Cloanlyst program. The automated inference of antibody clonality was followed up by visual inspection of the DNA sequence alignments for confirmation. The heavy and light chain gene sequences from the sorted B cells or inferred UCA and IAs were commercially generated and used to express purified recombinant mAbs as described (88). Heavy and light chain immunoglobulin repertoire next-generation sequencing of monkey RM6072 was performed with the Illumina MiSeq platform using primers targeting the VH1 and V κ 2 families to identify DH650 clonal members using a previously described protocol (23, 103). For mAb isolation from RM5695, bulk cDNA was synthesized from the five neutralization-positive B cell culture wells using random hexamers as previously described (104). Subsequently, immunoglobulin heavy chain (IgG) and light chain (IgK and IgL) variable regions were separately amplified by nested PCR cycles using pools of rhesus macaque primers as previously described (105). Sequences were analyzed using Cloanlyst (102) to infer putative variable region germline genes and identify clonal lineages. The heavy and lambda chain variable regions of the RM5695 lineage were codon optimized, synthesized with a murine immunoglobulin signal peptide (tripeptide sequence VHS) immediately preceding the 5' end of FRW1, and cloned into rhesus IgG1 (RhCMV-H) and IgL (RhCMV-L) expression vectors directly upstream of the respective constant regions using AgeI/NheI and AgeI/ScaI restriction sites, respectively (105). Recombinant mAbs were expressed by cotransfection of paired heavy and lambda chain plasmids into 293Freestyle cells as previously described (93), purified from cell supernatant using the Protein A/Protein G GraviTrap kit (GE Healthcare), and buffer-exchanged into PBS.

Next-generation sequencing of naïve B cells and IgDiscover analysis

PBMCs isolated from RM5695 plasma obtained at week 48 after infection were stained with

LIVE/DEAD Aqua, CD3-PerCP-Cy55, CD4-BV785, CD8-BV711, CD14-PE-Cy7, CD20-BV605, IgD-FITC, IgG-Ax680, and IgM-BV650. Approximately 300,000 naïve B cells (CD20⁺, IgG⁻, IgD⁺, IgM⁺) were bulk sorted into RPMI with 10% FBS and 1% Pen-Strep using a BD FACSAria II. Total RNA was extracted using RNeasy RT per the manufacturer's guidelines (Molecular Research Center, Inc). Reverse transcription of mRNA transcripts, IgM and IgL variable region library preparation, and next-generation sequencing were performed as previously described (106), as these methods can be efficiently used for both humans and RMs. Both heavy and lambda immunoglobulin libraries were sequenced on Illumina MiSeq with 2 × 300 bp runs using the MiSeq Reagent V3 kit (600-cycle). Filtered, quality-controlled IgM and IgL sequences were analyzed using IgDiscover (57) to curate a personalized immunoglobulin repertoire library for RM5695. A naïve IgK variable region library was not prepared, because the RM5695 lineage uses a lambda chain. IgDiscover can identify functional VH, VL, VK, JH, JL, and JK genes, and denotes any novel genes and/or alleles with respect to the provided reference database. For this analysis, a recently published RM database was used as the template (21). The resulting personalized database was then used in SONAR (107) to accurately assign germline immunoglobulin genes and precisely determine somatic hypermutation frequencies for the RHA1.V2 lineage.

Auto- and polyreactivity analysis

RHA1.V2.01 mAb reactivity to nine autoantigens was measured using the AtheNA Multi-Lyte ANA kit (Zeus scientific, Inc, #A21101). Antibodies were twofold serially diluted starting at 50 µg/ml, and kit methods were followed per manufacturer's instructions. Samples were analyzed using AtheNA software. Indirect immunofluorescence binding of RHA1.V2.01 mAb to human epithelial (HEp-2) cells (Zeus Scientific, Somerville, NJ) was also performed per manufacturer's instructions. Briefly, 20 µl of diluted antibody (50 µg/ml) was added to antinuclear antibody (ANA) test slides. Slides were incubated for 20 min at room temperature in a humid chamber and then washed with 1X PBS. Goat-anti-rhesus Ig-FITC (Southern Biotech, Birmingham, AL) secondary antibody was added at a concentration of 30 µg/ml to each well. The slides were incubated for 20 min, washed twice, dried, fixed with 33% glycerol and cover-slipped. Slides were imaged using an Olympus AX70 microscope with a SpotFlex FX1520 camera. Images were acquired on a 40× objective using the FITC fluorescence channel. Positivity was determined by comparison with positive and negative control nonhuman primate mAbs DH1037 and DH570.30, respectively. Staining patterns were identified using the Zeus Scientific pattern guide.

Hierarchical clustering of RHA1.V2.01 and other V2 apex bNAb profiles

We used the Heatmap webtool at the Los Alamos HIV database (www.hiv.lanl.gov/content/sequence/HEATMAP/heatmap.html) (93, 106, 107). Input data were log₁₀ transformed IC₅₀ titers for RHA1.V2.01 and other V2 apex bNAbs for the 208 virus panel. For clustering, Euclidean distances and the Ward algorithm (108) were used. Bootstraps were calculated using 1000 iterations.

Neutralization signature analyses

These analyses were performed using the webtool GenSig (www.hiv.lanl.gov/content/sequence/GENETICSIGNATURES/gs.html) (59) as described in (60). Briefly, IC₅₀ titers for RM5695 RHA1.V2.01 and other V2 apex bNAbs, together with Env sequences from the 208-strain virus panel, were used as inputs. Two statistical strategies were used: (i) Fisher's test with a binary phenotype, IC₅₀ titer above or below the threshold (resistant and sensitive, respectively), and (ii) Wilcoxon test that compares distribution of IC₅₀ titers with and without a feature. The latter analyses were conducted two ways, including and excluding resistant viruses. In both strategies, every amino acid and glycan at each site were tested for associations, with and without a phylogenetic correction. A relaxed multiple test false discovery rate (FDR) (q -value < 0.2) was used to first filter all possible hypothetical associations. At this high threshold, several phylogenetically uncorrected signatures were found, raising the suspicion that phylogenetic artifacts could be at play. However, some of these signatures could be relevant and underlie the clade-specific sensitivity and/or resistance of the bNAb in question. Thus, to down-select the most statistically robust and relevant signature sites, each selected site was required to meet at least two of the following three criteria: (i) contact site (as defined below), (ii) at least one phylogenetically corrected signature, and (iii) at least one strong signature at $q < 0.1$. All associations with $q < 0.2$ at selected sites were used to identify sequence features associated with sensitivity or resistance to the bNAb. The Wilcoxon signatures did not identify any new sites or associations. Env contact sites were defined using the cryo-EM structure of PGT145 in complex with Env trimer [Protein Data Bank (PDB) ID 5V8L] and a cutoff of 8.5 Å from any antibody heavy atom (HXB2 positions: 120, 121, 122, 123, 124, 125, 126, 127, 128, 129, 130, 156, 157, 158, 159, 160, 161, 162, 163, 164, 165, 166, 167, 168, 169, 170, 171, 172, 173, 174, 175, 184, 191, 192, 200, 201, 305, 306, 307, 308, 309, 312, 313, 314, 315, and 321).

Soluble HIV-1 envelope trimer generation

HIV Env trimer BG505 DS-SOSIP.664 was produced in transiently transfected 293F cells

as previously described (109, 110). Briefly, the plasmid encoding the SOSIP trimer and a plasmid encoding furin were mixed at 4:1 ratio and transfected into 293F cells at 0.75 mg plasmid per 1 L cells (1.5×10^6 /ml) using 293Fectin (ThermoFisher) or Turbo293 transfection reagent (Speed BioSystems). Cells were then incubated in a shaker at 120 rpm, 37°C, 9% CO₂. The following day, 80 ml HyClone SFM4HEK293 medium and 20 ml FreeStyle 293 Expression Medium were added to each liter of cells. Env trimer protein was purified from the day-7 supernatant with VRC01 affinity chromatography, followed by gel filtration on a Sephadex200 16/60HL column and V3-exposed trimers were removed with negative selection on a 447-52D affinity column. The antigenicity of the trimers was confirmed with a panel of antibodies in the Meso Scale Discovery (MSD) platform.

Antibody Fab preparation

Variable regions of the RHA1.V2.01 antibody heavy and light chain genes were synthesized (Genscript) and subcloned into the pVRC8400 vector, in which a HRV3C cleavage site was inserted in the heavy-chain hinge region. The heavy and light chain pair was cotransfected in Expi293F cells (ThermoFisher) using Turbo293 transfection reagent (Speed BioSystems) as described previously (111). The culture supernatant was harvested 6 days after transfection and loaded on a protein A column, the column was washed with PBS, and IgG proteins were eluted with a low pH buffer. The eluted IgG proteins were cleaved by HRV3C, and the cleavage mixture was passed through a protein A column.

Cryo-EM data collection and processing

Antibody Fab fragments of RHA1.V2.01 were incubated with BG505 DS-SOSIP with the Fab in molar excess. At a 1 mg/ml concentration, 2.3 μ l of the complex was deposited on a C-flat grid (www.protochips.com). An FEI Vitrobot Mark IV was used to vitrify the grid with a wait time of 30 s, blot time of 3 s, and blot force of 1. Automated data collection was performed with Leginon (112) on a Titan Krios electron microscope equipped with a Gatan K2 Summit direct detection device. Exposures were taken in movie mode for 10 s with the total dose of 71.06 e⁻/Å² fractionated over 50 raw frames. Images were preprocessed through Appion (113, 114); MotionCor2 (115) was used for frame alignment and dose weighting. The CTF was determined using CTFFind4 (116, 117). Initial particle picking was done with DoG Picker (113, 114). RELION (118) was then used for particle extraction. CryoSPARC 2.12 (119) was used for two-dimensional (2D) classifications, ab initio 3D reconstruction, homogeneous refinement, and nonuniform 3D refinement. Initial 3D reconstruction was performed using

C1 symmetry, confirming one Fab per trimer, and C1 symmetry was applied for the final reconstruction and refinement. Coordinates from PDB ID 6NNF (120) and 6CA6 (58) were used for initial fit to the reconstructed map. Simulated annealing was performed on the first refinement followed by iterative manual fitting and real space refinement in Phenix (121) and Coot (122). Geometry and map fitting were evaluated throughout the process using Molprobit (123) and EMRinger (124). PyMOL (www.pymol.org) was used to generate figures.

Expression and crystallization of CH505 gp120:DH650 Fab complex

CH505 gp120 core (residues 44 to 492, Δ V1-V2 and Δ V3) (125) was expressed in HEK293S GnTI⁻ cells and purified by affinity chromatography on *Galanthus nivalis* lectin (Vector Laboratories) followed by gel filtration on Superdex 200 column (GE). Deglycosylation was carried out with endoglycosidase H (endoH; New England Biolabs) in deglycosylation buffer (50 mM sodium acetate, pH 6, 5 mM EDTA, 500 mM NaCl, 10 μ l endoH, 1 μ g/ μ l leupeptin, 1 μ g/ μ l aprotinin) at 37°C overnight, followed by buffer exchange to 40 mM Tris HCl, pH 7.4, 1 M NaCl, 2 mM MnCl₂, 2 mM CaCl₂, and passage through a concanavalin A column (Sigma) to remove any gp120 that had not been fully deglycosylated by the endoH treatment. The eluate was buffer exchanged by passage over a Superdex200 column (GE) into 2.5mM Tris-HCl pH7.5, 350mM NaCl, followed by concentration to 4 mg/ml. The Fab fragment of mAb DH650 was expressed in HEK293T cells, as described in (125). DH650-gp120 core complex was formed by incubating gp120 core with DH650 in 1:1.3 molar ratio followed by gel filtration on Superdex 200 (GE) column in buffer 2.5 mM Tris-HCl pH 7.5, 350 mM NaCl. The complex was concentrated to 8.5 mg/ml and crystallized by hanging-drop vapor diffusion in 20% PEG 8K, 100 mM Tris pH 8, 500 mM NaCl.

Determination of CH505 gp120:DH650 Fab crystal structure

X-ray diffraction data to 2.8-Å resolution were collected at the Advanced Photon Source (Argonne National Laboratories) on NE-CAT beamline 24-ID-C. Intensity data were integrated, scaled, and merged with XDS and XSCALE (126) (see table S4). An initial model, obtained by molecular replacement with Phaser (127) using the ZM176.6 gp120 core (PDB ID 4LST), was rebuilt and refined with COOT (128) and Buster (Global Phasing, Ltd., Cambridge, UK), respectively. The final model (PDB ID 6XCJ) includes residues 52 to 128, 207 to 299, 327 to 396, and 409 to 488 of CH505 gp120, heavy chain residues 1 to 223, and light chain residues 1 to 219 of Fab DH650.

Negative-stain electron microscopy of CH505 SOSIP:DH650 Fab complex

CH505 DS-SOSIP, prepared as described in (7), was mixed with a DH650 Fab in a 1:4 molar ratio. After incubation for 1 hour, the complex was loaded on a Superose 6 column (GE). The SOSIP-Fab complex was diluted to 0.1 mg/ml and applied to freshly glow-discharged, carbon-coated EM grids and negatively stained with 1% uranyl formate. Images were recorded on an FEI Tecnai T12 electron microscope, operated at 120 kV, and equipped with a charge-coupled detector. Particles were selected and class averages computed with EMAN2 (129).

Neutralization fingerprint

The neutralization fingerprint of a monoclonal antibody is defined as the potency pattern with which the antibody neutralizes a set of diverse viral strains. The neutralization fingerprints of V2 targeting bNAbs, including VRC26, PGT145, PG9, and VRC38 classes, as well as a set of other HIV-1 bNAbs were compared and clustered according to fingerprint similarity, as described previously (59), using a panel of 208 HIV-1 viral strains.

Statistical analyses

Statistical tests were calculated by using GraphPad Prism 7 software. The Mann-Whitney test was used to determine whether the viral loads (peak and set point) of anti-CD8 treated animals were significantly different from untreated animals and whether viral loads (peak and set point) were greater in animals that developed bNAbs compared with those that did not. We chose a nonparametric rank-based test because both peak and set point viral loads of the untreated group and the bNAb and non-bNAb groups failed the D'Agostino and Pearson normality test ($P < 0.05$). The Spearman's rank correlation test was used to determine whether there is a significant correlation between set point viral loads and autologous tier 2 NAb titers. The geometric means were calculated using the Column statistics function of GraphPad Prism. The Chi-squared test was used on 2 × 2 contingency tables of shared and nonshared mutations within or between groups of humans and animals infected by viruses bearing the same (homologous) or different (heterologous) Envs to determine whether Env residue mutations demonstrated significant strain specificity. Separate tests were run to analyze total shared and nonshared mutations for the groups overall and for any discordant CH505, CH848, or CAP256SU group pairing.

Data and software availability

GenBank accession numbers for all HIV-1 env sequences analyzed in this study are as follows: MN471655-MN472016, MT484339-MT487491, MT580365-MT580445, MT509359, GQ999989, HQ625604, KC863461-KC863464, KP241776,

KF996577-KF996601, KF996604, KF996606, KF996610-KF996630, KF996632-KF996662, KF996664-KF996678, KF996680, KF996682-KF996683, KF996685-KF996716, KF698223-KT698227, MF572809-MF572829, ET203980-EF203981, and MK205498-MK205507. HIV-1 Env sequences from the human subject CAP256 were previously published (3, 5, 130). GenBank accession numbers for immunoglobulin genes are: MT581213-MT581268, MT610888-MT610895, and MT656172-MT656253. Cryo-EM maps and fitted coordinates have been deposited with database codes EMDB-22295 and PDB ID 6XRT, respectively. DH650 bound to the gp120 core was deposited with database code PDB ID 6XCJ.

REFERENCES AND NOTES

- B. F. Keele *et al.*, Identification and characterization of transmitted and early founder virus envelopes in primary HIV-1 infection. *Proc. Natl. Acad. Sci. U.S.A.* **105**, 7552–7557 (2008). doi: [10.1073/pnas.0802203105](https://doi.org/10.1073/pnas.0802203105); pmid: [18490657](https://pubmed.ncbi.nlm.nih.gov/18490657/)
- H. X. Liao *et al.*, Co-evolution of a broadly neutralizing HIV-1 antibody and founder virus. *Nature* **496**, 469–476 (2013). doi: [10.1038/nature12053](https://doi.org/10.1038/nature12053); pmid: [23552890](https://pubmed.ncbi.nlm.nih.gov/23552890/)
- N. A. Doria-Rose *et al.*, Developmental pathway for potent HIV-2-directed HIV-neutralizing antibodies. *Nature* **509**, 55–62 (2014). doi: [10.1038/nature13036](https://doi.org/10.1038/nature13036); pmid: [24590074](https://pubmed.ncbi.nlm.nih.gov/24590074/)
- F. Gao *et al.*, Cooperation of B cell lineages in induction of HIV-1-broadly neutralizing antibodies. *Cell* **158**, 481–491 (2014). doi: [10.1016/j.cell.2014.06.022](https://doi.org/10.1016/j.cell.2014.06.022); pmid: [25065977](https://pubmed.ncbi.nlm.nih.gov/25065977/)
- J. N. Bhiman *et al.*, Viral variants that initiate and drive maturation of HIV-2-directed HIV-1 broadly neutralizing antibodies. *Nat. Med.* **21**, 1332–1336 (2015). doi: [10.1038/nm.3963](https://doi.org/10.1038/nm.3963); pmid: [26457756](https://pubmed.ncbi.nlm.nih.gov/26457756/)
- M. Bonsignori *et al.*, Maturation pathway from germline to broad HIV-1 neutralizer of a CD4-mimic antibody. *Cell* **165**, 449–463 (2016). doi: [10.1016/j.cell.2016.02.022](https://doi.org/10.1016/j.cell.2016.02.022); pmid: [26949186](https://pubmed.ncbi.nlm.nih.gov/26949186/)
- M. Bonsignori *et al.*, Staged induction of HIV-1 glycan-dependent broadly neutralizing antibodies. *Sci. Transl. Med.* **9**, eaai7514 (2017). doi: [10.1126/scitranslmed.aai7514](https://doi.org/10.1126/scitranslmed.aai7514); pmid: [28298420](https://pubmed.ncbi.nlm.nih.gov/28298420/)
- E. Landais *et al.*, HIV envelope glycoform heterogeneity and localized diversity govern the initiation and maturation of a V2 apex broadly neutralizing antibody lineage. *Immunity* **47**, 990–1003.e9 (2017). doi: [10.1016/j.immuni.2017.11.002](https://doi.org/10.1016/j.immuni.2017.11.002); pmid: [29166592](https://pubmed.ncbi.nlm.nih.gov/29166592/)
- H. Li *et al.*, Envelope residue 375 substitutions in simian-human immunodeficiency viruses enhance CD4 binding and replication in rhesus macaques. *Proc. Natl. Acad. Sci. U.S.A.* **113**, E3413–E3422 (2016). doi: [10.1073/pnas.1606636113](https://doi.org/10.1073/pnas.1606636113); pmid: [27247400](https://pubmed.ncbi.nlm.nih.gov/27247400/)
- P. D. Kwong, J. R. Mascola, HIV-1 vaccines based on antibody identification, B cell ontogeny, and epitope structure. *Immunity* **48**, 855–871 (2018). doi: [10.1016/j.immuni.2018.04.029](https://doi.org/10.1016/j.immuni.2018.04.029); pmid: [29768174](https://pubmed.ncbi.nlm.nih.gov/29768174/)
- D. Sok, D. R. Burton, Recent progress in broadly neutralizing antibodies to HIV. *Nat. Immunol.* **19**, 1179–1188 (2018). doi: [10.1038/s41590-018-0235-7](https://doi.org/10.1038/s41590-018-0235-7); pmid: [30333615](https://pubmed.ncbi.nlm.nih.gov/30333615/)
- B. F. Haynes *et al.*, Cardiophilin polyspecific autoreactivity in two broadly neutralizing HIV-1 antibodies. *Science* **308**, 1906–1908 (2005). doi: [10.1126/science.1111781](https://doi.org/10.1126/science.1111781); pmid: [15860590](https://pubmed.ncbi.nlm.nih.gov/15860590/)
- G. Y. Chuang *et al.*, Structural survey of broadly neutralizing antibodies targeting the HIV-1 Env trimer delineates epitope categories and characteristics of recognition. *Structure* **27**, 196–206.e6 (2019). doi: [10.1016/j.str.2018.10.007](https://doi.org/10.1016/j.str.2018.10.007); pmid: [30471922](https://pubmed.ncbi.nlm.nih.gov/30471922/)
- E. C. Holmes, Error thresholds and the constraints to RNA virus evolution. *Trends Microbiol.* **11**, 543–546 (2003). doi: [10.1016/j.tim.2003.10.006](https://doi.org/10.1016/j.tim.2003.10.006); pmid: [14659685](https://pubmed.ncbi.nlm.nih.gov/14659685/)
- J. Woo, D. L. Robertson, S. C. Lovell, Constraints on HIV-1 diversity from protein structure. *J. Virol.* **84**, 12995–13003 (2010). doi: [10.1128/JVI.00702-10](https://doi.org/10.1128/JVI.00702-10); pmid: [20881050](https://pubmed.ncbi.nlm.nih.gov/20881050/)
- H. K. Haddox, A. S. Dingens, J. D. Bloom, Experimental estimation of the effects of all amino-acid mutations to HIV's envelope protein on viral replication in cell culture. *PLoS Pathog.* **12**, e1006114 (2016). doi: [10.1371/journal.ppat.1006114](https://doi.org/10.1371/journal.ppat.1006114); pmid: [27959955](https://pubmed.ncbi.nlm.nih.gov/27959955/)
- R. Wyatt *et al.*, The antigenic structure of the HIV gp120 envelope glycoprotein. *Nature* **393**, 705–711 (1998). doi: [10.1038/31514](https://doi.org/10.1038/31514); pmid: [9641684](https://pubmed.ncbi.nlm.nih.gov/9641684/)
- X. Wei *et al.*, Antibody neutralization and escape by HIV-1. *Nature* **422**, 307–312 (2003). doi: [10.1038/nature01470](https://doi.org/10.1038/nature01470); pmid: [12646921](https://pubmed.ncbi.nlm.nih.gov/12646921/)
- B. R. Starcich *et al.*, Identification and characterization of conserved and variable regions in the envelope gene of HTLV-III/LAV, the retrovirus of AIDS. *Cell* **45**, 637–648 (1986). doi: [10.1016/0092-8674\(86\)90778-6](https://doi.org/10.1016/0092-8674(86)90778-6); pmid: [2423250](https://pubmed.ncbi.nlm.nih.gov/2423250/)
- P. D. Kwong *et al.*, HIV-1 evades antibody-mediated neutralization through conformational masking of receptor-binding sites. *Nature* **420**, 678–682 (2002). doi: [10.1038/nature01188](https://doi.org/10.1038/nature01188); pmid: [12478295](https://pubmed.ncbi.nlm.nih.gov/12478295/)
- A. Ramesh *et al.*, Structure and diversity of the rhesus macaque immunoglobulin loci through multiple de novo genome assemblies. *Front. Immunol.* **8**, 1407 (2017). doi: [10.3389/fimmu.2017.01407](https://doi.org/10.3389/fimmu.2017.01407); pmid: [29163486](https://pubmed.ncbi.nlm.nih.gov/29163486/)
- P. L. Moore *et al.*, Multiple pathways of escape from HIV broadly cross-neutralizing V2-dependent antibodies. *J. Virol.* **87**, 4882–4894 (2013). doi: [10.1128/JVI.03424-12](https://doi.org/10.1128/JVI.03424-12); pmid: [23408621](https://pubmed.ncbi.nlm.nih.gov/23408621/)
- W. B. Williams *et al.*, Initiation of HIV neutralizing B cell lineages with sequential envelope immunizations. *Nat. Commun.* **8**, 1732 (2017). doi: [10.1038/s41467-017-01336-3](https://doi.org/10.1038/s41467-017-01336-3); pmid: [29170366](https://pubmed.ncbi.nlm.nih.gov/29170366/)
- Z. M. Ndhlovu *et al.*, Magnitude and kinetics of CD8⁺ T Cell activation during hyperacute HIV infection impact viral set point. *Immunity* **43**, 591–604 (2015). doi: [10.1016/j.immuni.2015.08.012](https://doi.org/10.1016/j.immuni.2015.08.012); pmid: [26362266](https://pubmed.ncbi.nlm.nih.gov/26362266/)
- M. L. Robb *et al.*, Prospective study of acute HIV-1 infection in adults in east Africa and Thailand. *N. Engl. J. Med.* **374**, 2120–2130 (2016). doi: [10.1056/NEJMoa1508952](https://doi.org/10.1056/NEJMoa1508952); pmid: [27192360](https://pubmed.ncbi.nlm.nih.gov/27192360/)
- M. S. Seaman *et al.*, Tiered categorization of a diverse panel of HIV-1 Env pseudoviruses for assessment of neutralizing antibodies. *J. Virol.* **84**, 1439–1452 (2010). doi: [10.1128/JVI.02108-09](https://doi.org/10.1128/JVI.02108-09); pmid: [19939925](https://pubmed.ncbi.nlm.nih.gov/19939925/)
- A. deCamp *et al.*, Global panel of HIV-1 Env reference strains for standardized assessments of vaccine-elicited neutralizing antibodies. *J. Virol.* **88**, 2489–2507 (2014). doi: [10.1128/JVI.02853-13](https://doi.org/10.1128/JVI.02853-13); pmid: [24352443](https://pubmed.ncbi.nlm.nih.gov/24352443/)
- P. Hraber *et al.*, Prevalence of broadly neutralizing antibody responses during chronic HIV-1 infection. *AIDS* **28**, 163–169 (2014). doi: [10.1097/QAD.0000000000001016](https://doi.org/10.1097/QAD.0000000000001016); pmid: [24361678](https://pubmed.ncbi.nlm.nih.gov/24361678/)
- HIV-1 strains 25710 and Q23.17 have been variably reported as tier 1b or tier 2 in neutralization sensitivity to different panels of heterologous HIV-1 positive plasma. In all studies, these two virus strains have been shown to be much closer to tier 2 viruses than to lab-adapted tier 1A viruses in their neutralization sensitivity patterns. See (26–28).
- J. M. Decker *et al.*, Antigenic conservation and immunogenicity of the HIV coreceptor binding site. *J. Exp. Med.* **201**, 1407–1419 (2005). doi: [10.1084/jem.20042510](https://doi.org/10.1084/jem.20042510); pmid: [15867093](https://pubmed.ncbi.nlm.nih.gov/15867093/)
- K. L. Davis *et al.*, Human immunodeficiency virus type 2 (HIV-2)/HIV-1 envelope chimeras detect high titers of broadly reactive HIV-1 V3-specific antibodies in human plasma. *J. Virol.* **83**, 1240–1259 (2009). doi: [10.1128/JVI.01743-08](https://doi.org/10.1128/JVI.01743-08); pmid: [19019969](https://pubmed.ncbi.nlm.nih.gov/19019969/)
- J. Chen *et al.*, Effect of the cytoplasmic domain on antigenic characteristics of HIV-1 envelope glycoprotein. *Science* **349**, 191–195 (2015). doi: [10.1126/science.aaa9804](https://doi.org/10.1126/science.aaa9804); pmid: [26113642](https://pubmed.ncbi.nlm.nih.gov/26113642/)
- E. Landais *et al.*, Broadly neutralizing antibody responses in a large longitudinal sub-Saharan HIV primary infection cohort. *PLoS Pathog.* **12**, e1005369 (2016). doi: [10.1371/journal.ppat.1005369](https://doi.org/10.1371/journal.ppat.1005369); pmid: [26766578](https://pubmed.ncbi.nlm.nih.gov/26766578/)
- E. Landais, P. L. Moore, Development of broadly neutralizing antibodies in HIV-1 infected elite neutralizers. *Retrovirology* **15**, 61 (2018). doi: [10.1186/s12977-018-0443-0](https://doi.org/10.1186/s12977-018-0443-0); pmid: [30185183](https://pubmed.ncbi.nlm.nih.gov/30185183/)
- H. J. Barbian *et al.*, Neutralization properties of simian immunodeficiency viruses infecting chimpanzees and gorillas. *mBio* **6**, e00296-15 (2015). doi: [10.1128/mBio.00296-15](https://doi.org/10.1128/mBio.00296-15); pmid: [25900654](https://pubmed.ncbi.nlm.nih.gov/25900654/)
- V. Sanchez-Merino *et al.*, Detection of broadly neutralizing activity within the first months of HIV-1 infection. *J. Virol.* **90**, 5231–5245 (2016). doi: [10.1128/JVI.00049-16](https://doi.org/10.1128/JVI.00049-16); pmid: [26984721](https://pubmed.ncbi.nlm.nih.gov/26984721/)
- N. Goonetilleke *et al.*, The first T cell response to transmitted/founder virus contributes to the control of acute viremia in HIV-1 infection. *J. Exp. Med.* **206**, 1253–1272 (2009). doi: [10.1084/jem.20090365](https://doi.org/10.1084/jem.20090365); pmid: [19487423](https://pubmed.ncbi.nlm.nih.gov/19487423/)
- J. F. Salazar-Gonzalez *et al.*, Genetic identity, biological phenotype, and evolutionary pathways of transmitted/founder viruses in acute and early HIV-1 infection. *J. Exp. Med.* **206**, 1273–1289 (2009). doi: [10.1084/jem.20090378](https://doi.org/10.1084/jem.20090378); pmid: [19487424](https://pubmed.ncbi.nlm.nih.gov/19487424/)
- K. J. Bar *et al.*, Early low-titer neutralizing antibodies impede HIV-1 replication and select for virus escape. *PLoS Pathog.* **8**, e1002721 (2012). doi: [10.1371/journal.ppat.1002721](https://doi.org/10.1371/journal.ppat.1002721); pmid: [22693447](https://pubmed.ncbi.nlm.nih.gov/22693447/)
- M. Markowitz *et al.*, A novel antiviral intervention results in more accurate assessment of human immunodeficiency virus type 1 replication dynamics and T-cell decay in vivo. *J. Virol.* **77**, 5037–5038 (2003). doi: [10.1128/JVI.77.8.5037-5038.2003](https://doi.org/10.1128/JVI.77.8.5037-5038.2003); pmid: [12663814](https://pubmed.ncbi.nlm.nih.gov/12663814/)
- D. D. Ho *et al.*, Rapid turnover of plasma virions and CD4 lymphocytes in HIV-1 infection. *Nature* **373**, 123–126 (1995). doi: [10.1038/373123a0](https://doi.org/10.1038/373123a0); pmid: [7816094](https://pubmed.ncbi.nlm.nih.gov/7816094/)
- X. Wei *et al.*, Viral dynamics in human immunodeficiency virus type 1 infection. *Nature* **373**, 117–122 (1995). doi: [10.1038/373117a0](https://doi.org/10.1038/373117a0); pmid: [7529365](https://pubmed.ncbi.nlm.nih.gov/7529365/)
- P. Borrow *et al.*, Antiviral pressure exerted by HIV-1-specific cytotoxic T lymphocytes (CTLs) during primary infection demonstrated by rapid selection of CTL escape virus. *Nat. Med.* **3**, 205–211 (1997). doi: [10.1038/nm0297-205](https://doi.org/10.1038/nm0297-205); pmid: [9018240](https://pubmed.ncbi.nlm.nih.gov/9018240/)
- P. Hraber *et al.*, Longitudinal antigenic sequences and sites from intra-host evolution (LASSIE) identifies immune-selected HIV variants. *Viruses* **7**, 5443–5475 (2015). doi: [10.3390/v7102881](https://doi.org/10.3390/v7102881); pmid: [26506369](https://pubmed.ncbi.nlm.nih.gov/26506369/)
- K. Wagh *et al.*, Completeness of HIV-1 envelope glycan shield at transmission determines neutralization breadth. *Cell Rep.* **25**, 893–908.e7 (2018). doi: [10.1016/j.celrep.2018.09.087](https://doi.org/10.1016/j.celrep.2018.09.087); pmid: [30355496](https://pubmed.ncbi.nlm.nih.gov/30355496/)
- J. M. Coffin, Structure, replication, and recombination of retrovirus genomes: Some unifying hypotheses. *J. Gen. Virol.* **42**, 1–26 (1979). doi: [10.1099/0022-1317-42-1-1](https://doi.org/10.1099/0022-1317-42-1-1); pmid: [215703](https://pubmed.ncbi.nlm.nih.gov/215703/)
- N. Wood *et al.*, HIV evolution in early infection: Selection pressures, patterns of insertion and deletion, and the impact of APOBEC. *PLoS Pathog.* **5**, e1000414 (2009). doi: [10.1371/journal.ppat.1000414](https://doi.org/10.1371/journal.ppat.1000414); pmid: [19424423](https://pubmed.ncbi.nlm.nih.gov/19424423/)
- B. M. Mavbakure *et al.*, Positive selection at key residues in the HIV envelope distinguishes broad and strain-specific plasma neutralizing antibodies. *J. Virol.* **93**, e01685-18 (2019). doi: [10.1128/JVI.01685-18](https://doi.org/10.1128/JVI.01685-18); pmid: [30567996](https://pubmed.ncbi.nlm.nih.gov/30567996/)
- N. A. Doria-Rose *et al.*, New member of the HIV-2-directed CAP256-VRC26 lineage that shows increased breadth and exceptional potency. *J. Virol.* **90**, 76–91 (2015). doi: [10.1128/JVI.01791-15](https://doi.org/10.1128/JVI.01791-15); pmid: [26468542](https://pubmed.ncbi.nlm.nih.gov/26468542/)
- K. O. Saunders *et al.*, Targeted selection of HIV-specific antibody mutations by engineering B cell maturation. *Science* **366**, eea7199 (2019). doi: [10.1126/science.aay7199](https://doi.org/10.1126/science.aay7199); pmid: [31806786](https://pubmed.ncbi.nlm.nih.gov/31806786/)
- R. Andrabi *et al.*, Identification of common features in prototype broadly neutralizing antibodies to HIV envelope V2 apex to facilitate vaccine design. *Immunity* **43**, 959–973 (2015). doi: [10.1016/j.immuni.2015.10.014](https://doi.org/10.1016/j.immuni.2015.10.014); pmid: [26588781](https://pubmed.ncbi.nlm.nih.gov/26588781/)
- J. Gorman *et al.*, Structures of HIV-1 Env V1V2 with broadly neutralizing antibodies reveal commonalities that enable vaccine design. *Nat. Struct. Mol. Biol.* **23**, 81–90 (2016). doi: [10.1038/nsmb.3144](https://doi.org/10.1038/nsmb.3144); pmid: [26689967](https://pubmed.ncbi.nlm.nih.gov/26689967/)
- J. Gorman *et al.*, Structure of super-potent antibody CAP256-VRC26.25 in complex with HIV-1 envelope reveals a combined mode of trimer-apex recognition. *Cell Rep.* **31**, 107488 (2020). doi: [10.1016/j.celrep.2020.03.052](https://doi.org/10.1016/j.celrep.2020.03.052); pmid: [32268107](https://pubmed.ncbi.nlm.nih.gov/32268107/)
- J. F. Scheid *et al.*, Sequence and structural convergence of broad and potent HIV antibodies that mimic CD4 binding. *Science* **333**, 1633–1637 (2011). doi: [10.1126/science.1207227](https://doi.org/10.1126/science.1207227); pmid: [21764753](https://pubmed.ncbi.nlm.nih.gov/21764753/)
- K. Wiehe *et al.*, Functional relevance of improbable antibody mutations for HIV broadly neutralizing antibody development. *Cell Host Microbe* **23**, 759–765.e6 (2018). doi: [10.1016/j.chom.2018.04.018](https://doi.org/10.1016/j.chom.2018.04.018); pmid: [29861171](https://pubmed.ncbi.nlm.nih.gov/29861171/)
- Z. Zhou *et al.*, Multidonor analysis reveals structural elements, genetic determinants, and maturation pathway for HIV-1 neutralization by VRC01-class antibodies. *Immunity* **39**, 245–258 (2013). doi: [10.1016/j.immuni.2013.04.012](https://doi.org/10.1016/j.immuni.2013.04.012); pmid: [23911655](https://pubmed.ncbi.nlm.nih.gov/23911655/)
- M. M. Corcoran *et al.*, Production of individualized V gene databases reveals high levels of immunoglobulin genetic diversity. *Nat. Commun.* **7**, 13642 (2016). doi: [10.1038/ncomms13642](https://doi.org/10.1038/ncomms13642); pmid: [27995928](https://pubmed.ncbi.nlm.nih.gov/27995928/)
- K. Rantalainen *et al.*, Co-evolution of HIV envelope and apex-targeting neutralizing antibody lineage provides

- benchmarks for vaccine design. *Cell Rep.* **23**, 3249–3261 (2018). doi: [10.1016/j.celrep.2018.05.046](https://doi.org/10.1016/j.celrep.2018.05.046); pmid: [29898396](https://pubmed.ncbi.nlm.nih.gov/29898396/)
59. I. S. Georgiev et al., Delineating antibody recognition in polyclonal sera from patterns of HIV-1 isolate neutralization. *Science* **340**, 751–756 (2013). doi: [10.1126/science.1233989](https://doi.org/10.1126/science.1233989); pmid: [23661761](https://pubmed.ncbi.nlm.nih.gov/23661761/)
60. C. A. Bricault et al., HIV-1 neutralizing antibody signatures and application to epitope-targeted vaccine design. *Cell Host Microbe* **25**, 59–72.e8 (2019). doi: [10.1016/j.chom.2018.12.001](https://doi.org/10.1016/j.chom.2018.12.001); pmid: [30629920](https://pubmed.ncbi.nlm.nih.gov/30629920/)
61. L. M. Walker et al., Rapid development of glycan-specific, broad, and potent anti-HIV-1 gp120 neutralizing antibodies in an R5 SHIV/HIV chimeric virus-infected macaque. *Proc. Natl. Acad. Sci. U.S.A.* **108**, 20125–20129 (2011). doi: [10.1073/pnas.1117531108](https://doi.org/10.1073/pnas.1117531108); pmid: [22123961](https://pubmed.ncbi.nlm.nih.gov/22123961/)
62. M. Jia, H. Lu, M. Markowitz, C. Cheng-Mayer, X. Wu, Development of broadly neutralizing antibodies and their mapping by monomeric gp120 in human immunodeficiency virus type 1-infected humans and simian-human immunodeficiency virus SHIVSF162P3N-infected macaques. *J. Virol.* **90**, 4017–4031 (2016). doi: [10.1128/JVI.02898-15](https://doi.org/10.1128/JVI.02898-15); pmid: [26842476](https://pubmed.ncbi.nlm.nih.gov/26842476/)
63. N. Gao et al., Development of broad neutralizing activity in simian/human immunodeficiency virus-infected rhesus macaques after long-term infection. *AIDS* **32**, 555–563 (2018). doi: [10.1097/QAD.0000000000001724](https://doi.org/10.1097/QAD.0000000000001724); pmid: [29239895](https://pubmed.ncbi.nlm.nih.gov/29239895/)
64. N. Gao et al., Development of antibodies with broad neutralization specificities against HIV-1 after long term SHIV infection in macaques. *Viruses* **12**, 163 (2020). doi: [10.3390/v12020163](https://doi.org/10.3390/v12020163); pmid: [32023860](https://pubmed.ncbi.nlm.nih.gov/32023860/)
65. H. X. Liao et al., Induction of antibodies in guinea pigs and rhesus monkeys against the human immunodeficiency virus type 1 envelope: Neutralization of nonpathogenic and pathogenic primary isolate simian/human immunodeficiency virus strains. *J. Virol.* **74**, 254–263 (2000). doi: [10.1128/JVI.74.1.254-263.2000](https://doi.org/10.1128/JVI.74.1.254-263.2000); pmid: [10590113](https://pubmed.ncbi.nlm.nih.gov/10590113/)
66. B. F. Haynes et al., Analysis of HIV-1 subtype B third variable region peptide motifs for induction of neutralizing antibodies against HIV-1 primary isolates. *Virology* **345**, 44–55 (2006). doi: [10.1016/j.virol.2005.08.042](https://doi.org/10.1016/j.virol.2005.08.042); pmid: [16242749](https://pubmed.ncbi.nlm.nih.gov/16242749/)
67. S. Wang et al., Polyvalent HIV-1 Env vaccine formulations delivered by the DNA priming plus protein boosting approach are effective in generating neutralizing antibodies against primary human immunodeficiency virus type 1 isolates from subtypes A, B, C, D and E. *Virology* **350**, 34–47 (2006). doi: [10.1016/j.virol.2006.02.032](https://doi.org/10.1016/j.virol.2006.02.032); pmid: [16616287](https://pubmed.ncbi.nlm.nih.gov/16616287/)
68. M. Pauthner et al., Elicitation of robust tier 2 neutralizing antibody responses in nonhuman primates by HIV envelope trimer immunization using optimized approaches. *Immunity* **46**, 1073–1088.e6 (2017). doi: [10.1016/j.immuni.2017.05.007](https://doi.org/10.1016/j.immuni.2017.05.007); pmid: [28636956](https://pubmed.ncbi.nlm.nih.gov/28636956/)
69. K. O. Saunders et al., Vaccine induction of heterologous tier 2 HIV-1 neutralizing antibodies in animal models. *Cell Rep.* **21**, 3681–3690 (2017). doi: [10.1016/j.celrep.2017.12.028](https://doi.org/10.1016/j.celrep.2017.12.028); pmid: [29281818](https://pubmed.ncbi.nlm.nih.gov/29281818/)
70. A. Torrents de la Peña et al., Immunogenicity in rabbits of HIV-1 SOSIP trimers from clades A, B, and C, given individually, sequentially, or in combination. *J. Virol.* **92**, e01957-17 (2018). doi: [10.1128/JVI.01957-17](https://doi.org/10.1128/JVI.01957-17); pmid: [29367243](https://pubmed.ncbi.nlm.nih.gov/29367243/)
71. R. Kong et al., Antibody lineages with vaccine-induced antigen-binding hotspots develop broad HIV neutralization. *Cell* **178**, 567–584.e19 (2019). doi: [10.1016/j.cell.2019.06.030](https://doi.org/10.1016/j.cell.2019.06.030); pmid: [31348886](https://pubmed.ncbi.nlm.nih.gov/31348886/)
72. P. J. Klasse, G. Ozorowski, R. W. Sanders, J. P. Moore, Env exceptionalism: Why are HIV-1 env glycoproteins atypical immunogens? *Cell Host Microbe* **27**, 507–518 (2020). doi: [10.1016/j.chom.2020.03.018](https://doi.org/10.1016/j.chom.2020.03.018); pmid: [32272076](https://pubmed.ncbi.nlm.nih.gov/32272076/)
73. Z. Wang et al., A broadly neutralizing macaque monoclonal antibody against the HIV-1 V3-Glycan patch. *eLife* **9**, e61991 (2020). doi: [10.7554/eLife.61991](https://doi.org/10.7554/eLife.61991); pmid: [33084569](https://pubmed.ncbi.nlm.nih.gov/33084569/)
74. B. F. Haynes, D. R. Burton, J. R. Mascola, Multiple roles for HIV broadly neutralizing antibodies. *Sci. Transl. Med.* **11**, eaaz2686 (2019). doi: [10.1126/scitranslmed.aaz2686](https://doi.org/10.1126/scitranslmed.aaz2686); pmid: [31666399](https://pubmed.ncbi.nlm.nih.gov/31666399/)
75. K. E. Stephenson, K. Wagh, B. Korber, D. H. Barouch, Vaccines and broadly neutralizing antibodies for HIV-1 prevention. *Annu. Rev. Immunol.* **38**, 673–703 (2020). doi: [10.1146/annurev-immunol-080219-023629](https://doi.org/10.1146/annurev-immunol-080219-023629); pmid: [32340576](https://pubmed.ncbi.nlm.nih.gov/32340576/)
76. A. Escolano et al., Immunization expands B cells specific to HIV-1 V3 glycan in mice and macaques. *Nature* **570**, 468–473 (2019). doi: [10.1038/s41586-019-1250-z](https://doi.org/10.1038/s41586-019-1250-z); pmid: [31142836](https://pubmed.ncbi.nlm.nih.gov/31142836/)
77. J. M. Steichen et al., A generalized HIV vaccine design strategy for priming of broadly neutralizing antibody responses. *Science* **366**, eaax4380 (2019). doi: [10.1126/science.aax4380](https://doi.org/10.1126/science.aax4380); pmid: [31672916](https://pubmed.ncbi.nlm.nih.gov/31672916/)
78. R. Pejchal et al., A potent and broad neutralizing antibody recognizes and penetrates the HIV glycan shield. *Science* **334**, 1097–1103 (2011). doi: [10.1126/science.1213256](https://doi.org/10.1126/science.1213256); pmid: [21998254](https://pubmed.ncbi.nlm.nih.gov/21998254/)
79. D. Sok et al., A prominent site of antibody vulnerability on HIV envelope incorporates a motif associated with CCR5 binding and its camouflaging glycans. *Immunity* **45**, 31–45 (2016). doi: [10.1016/j.immuni.2016.06.026](https://doi.org/10.1016/j.immuni.2016.06.026); pmid: [27438765](https://pubmed.ncbi.nlm.nih.gov/27438765/)
80. J. P. Julien et al., Broadly neutralizing antibody PGT121 allosterically modulates CD4 binding via recognition of the HIV-1 gp120 V3 base and multiple surrounding glycans. *PLoS Pathog.* **9**, e1003342 (2013). doi: [10.1371/journal.ppat.1003342](https://doi.org/10.1371/journal.ppat.1003342); pmid: [23658524](https://pubmed.ncbi.nlm.nih.gov/23658524/)
81. B. F. Haynes, G. Kelseo, S. C. Harrison, T. B. Kepler, B-cell-lineage immunogen design in vaccine development with HIV-1 as a case study. *Nat. Biotechnol.* **30**, 423–433 (2012). doi: [10.1038/nbt.2197](https://doi.org/10.1038/nbt.2197); pmid: [22565972](https://pubmed.ncbi.nlm.nih.gov/22565972/)
82. P. L. Moore, The neutralizing antibody response to the HIV-1 env protein. *Curr. HIV Res.* **16**, 21–28 (2018). doi: [10.2174/1570162X15666171124122044](https://doi.org/10.2174/1570162X15666171124122044); pmid: [29173180](https://pubmed.ncbi.nlm.nih.gov/29173180/)
83. M. Sarzotti-Kelseo et al., Optimization and validation of the TZM-bl assay for standardized assessments of neutralizing antibodies against HIV-1. *J. Immunol. Methods* **409**, 131–146 (2014). doi: [10.1016/j.jim.2013.11.022](https://doi.org/10.1016/j.jim.2013.11.022); pmid: [24291345](https://pubmed.ncbi.nlm.nih.gov/24291345/)
84. Q. Han et al., Difficult-to-neutralize global HIV-1 isolates are neutralized by antibodies targeting open envelope conformations. *Nat. Commun.* **10**, 2898 (2019). doi: [10.1038/s41467-019-10899-2](https://doi.org/10.1038/s41467-019-10899-2); pmid: [31263112](https://pubmed.ncbi.nlm.nih.gov/31263112/)
85. L. D. Williams et al., Potent and broad HIV-neutralizing antibodies in memory B cells and plasma. *Sci. Immunol.* **2**, eaal2200 (2017). doi: [10.1126/sciimmunol.aal2200](https://doi.org/10.1126/sciimmunol.aal2200); pmid: [28783671](https://pubmed.ncbi.nlm.nih.gov/28783671/)
86. S. M. Alam et al., Antigenicity and immunogenicity of RV144 vaccine AIDSVAX clade E envelope immunogen is enhanced by a gp120 N-terminal deletion. *J. Virol.* **87**, 1554–1568 (2013). doi: [10.1128/JVI.00718-12](https://doi.org/10.1128/JVI.00718-12); pmid: [23175357](https://pubmed.ncbi.nlm.nih.gov/23175357/)
87. S. M. Alam et al., Mimicry of an HIV broadly neutralizing antibody epitope with a synthetic glycopeptide. *Sci. Transl. Med.* **9**, eaai7521 (2017). doi: [10.1126/scitranslmed.aai7521](https://doi.org/10.1126/scitranslmed.aai7521); pmid: [28298421](https://pubmed.ncbi.nlm.nih.gov/28298421/)
88. H. X. Liao et al., High-throughput isolation of immunoglobulin genes from single human B cells and expression as monoclonal antibodies. *J. Virol. Methods* **158**, 171–179 (2009). doi: [10.1016/j.jviro.2009.02.014](https://doi.org/10.1016/j.jviro.2009.02.014); pmid: [19428587](https://pubmed.ncbi.nlm.nih.gov/19428587/)
89. M. Bonsignori et al., Analysis of a clonal lineage of HIV-1 envelope V2/V3 conformational epitope-specific broadly neutralizing antibodies and their inferred unmutated common ancestors. *J. Virol.* **85**, 9998–10009 (2011). doi: [10.1128/JVI.05045-11](https://doi.org/10.1128/JVI.05045-11); pmid: [21795340](https://pubmed.ncbi.nlm.nih.gov/21795340/)
90. M. Blasi et al., IDLV-HIV-1 Env vaccination in non-human primates induces affinity maturation of antigen-specific memory B cells. *Commun. Biol.* **1**, 134 (2018). doi: [10.1038/s42003-018-0131-6](https://doi.org/10.1038/s42003-018-0131-6); pmid: [30272013](https://pubmed.ncbi.nlm.nih.gov/30272013/)
91. M. A. Moody et al., HIV-1 gp120 vaccine induces affinity maturation in both new and persistent antibody clonal lineages. *J. Virol.* **86**, 7496–7507 (2012). doi: [10.1128/JVI.00426-12](https://doi.org/10.1128/JVI.00426-12); pmid: [22553329](https://pubmed.ncbi.nlm.nih.gov/22553329/)
92. K. Wiehe et al., Antibody light-chain-restricted recognition of the site of immune pressure in the RV144 HIV-1 vaccine trial is phylogenetically conserved. *Immunity* **41**, 909–918 (2014). doi: [10.1016/j.immuni.2014.11.014](https://doi.org/10.1016/j.immuni.2014.11.014); pmid: [25526306](https://pubmed.ncbi.nlm.nih.gov/25526306/)
93. X. Wu et al., Rational design of envelope identifies broadly neutralizing human monoclonal antibodies to HIV-1. *Science* **329**, 856–861 (2010). doi: [10.1126/science.1187659](https://doi.org/10.1126/science.1187659); pmid: [20616233](https://pubmed.ncbi.nlm.nih.gov/20616233/)
94. D. C. Montefiori, Evaluating neutralizing antibodies against HIV, SIV, and SHIV in luciferase reporter gene assays. *Curr. Protoc. Immunol.* **64**, 12.11.1–12.11.17 (2005). pmid: [18432938](https://pubmed.ncbi.nlm.nih.gov/18432938/)
95. S. P. Perletto et al., Amine-reactive dyes for dead cell discrimination in fixed samples. *Curr. Protoc. Cytom.* **53**, 9.34.1–9.34.14 (2010). doi: [10.1002/0471142956.cy0934a53](https://doi.org/10.1002/0471142956.cy0934a53); pmid: [20578108](https://pubmed.ncbi.nlm.nih.gov/20578108/)
96. M. M. Donaldson et al., Optimization and qualification of an 8-color intracellular cytokine staining assay for quantifying T cell responses in rhesus macaques for pre-clinical vaccine studies. *J. Immunol. Methods* **386**, 10–21 (2012). doi: [10.1016/j.jim.2012.08.011](https://doi.org/10.1016/j.jim.2012.08.011); pmid: [22955212](https://pubmed.ncbi.nlm.nih.gov/22955212/)
97. J. Huang et al., Isolation of human monoclonal antibodies from peripheral blood B cells. *Nat. Protoc.* **8**, 1907–1915 (2013). doi: [10.1038/nprot.2013.117](https://doi.org/10.1038/nprot.2013.117); pmid: [24030440](https://pubmed.ncbi.nlm.nih.gov/24030440/)
98. N. Doria-Rose et al., High throughput HIV-1 microneutralization assay. *Protoc. Exp. Biol.* **10**, 10138/protex.2013.069 (2013). doi: [10.1038/protex.2013.069](https://doi.org/10.1038/protex.2013.069)
99. K. Smith et al., Rapid generation of fully human monoclonal antibodies specific to a vaccinating antigen. *Nat. Protoc.* **4**, 372–384 (2009). doi: [10.1038/nprot.2009.3](https://doi.org/10.1038/nprot.2009.3); pmid: [19247287](https://pubmed.ncbi.nlm.nih.gov/19247287/)
100. B. Ewing, L. Hillier, M. C. Wendt, P. Green, Base-calling of automated sequencer traces using phred. I. Accuracy assessment. *Genome Res.* **8**, 175–185 (1998). doi: [10.1101/gr.8.3.175](https://doi.org/10.1101/gr.8.3.175); pmid: [9521921](https://pubmed.ncbi.nlm.nih.gov/9521921/)
101. J. M. Volpe, L. G. Cowell, T. B. Kepler, SoDA: Implementation of a 3D alignment algorithm for inference of antigen receptor recombinations. *Bioinformatics* **22**, 438–444 (2006). doi: [10.1093/bioinformatics/btk004](https://doi.org/10.1093/bioinformatics/btk004); pmid: [16357034](https://pubmed.ncbi.nlm.nih.gov/16357034/)
102. T. B. Kepler et al., Reconstructing a B-cell clonal lineage. II. Mutation, selection, and affinity maturation. *Front. Immunol.* **5**, 170 (2014). doi: [10.3389/fimmu.2014.00170](https://doi.org/10.3389/fimmu.2014.00170); pmid: [24795717](https://pubmed.ncbi.nlm.nih.gov/24795717/)
103. R. Zhang et al., Initiation of immune tolerance-controlled HIV gp41 neutralizing B cell lineages. *Sci. Transl. Med.* **8**, 336ra62 (2016). doi: [10.1126/scitranslmed.aaf0618](https://doi.org/10.1126/scitranslmed.aaf0618); pmid: [27122615](https://pubmed.ncbi.nlm.nih.gov/27122615/)
104. T. Tiller et al., Efficient generation of monoclonal antibodies from single human B cells by single cell RT-PCR and expression vector cloning. *J. Immunol. Methods* **329**, 112–124 (2008). doi: [10.1016/j.jim.2007.09.017](https://doi.org/10.1016/j.jim.2007.09.017); pmid: [17996249](https://pubmed.ncbi.nlm.nih.gov/17996249/)
105. D. Mason et al., Targeted isolation of antibodies directed against major sites of HIV Env vulnerability. *PLoS Pathog.* **12**, e1005537 (2016). doi: [10.1371/journal.ppat.1005537](https://doi.org/10.1371/journal.ppat.1005537); pmid: [27064278](https://pubmed.ncbi.nlm.nih.gov/27064278/)
106. S. J. Krebs et al., Longitudinal analysis reveals early development of three MPER-directed neutralizing antibody lineages from an HIV-1-infected individual. *Immunity* **50**, 677–691.e13 (2019). doi: [10.1016/j.immuni.2019.02.008](https://doi.org/10.1016/j.immuni.2019.02.008); pmid: [30876875](https://pubmed.ncbi.nlm.nih.gov/30876875/)
107. C. A. Schramm et al., SONAR: A high-throughput pipeline for inferring antibody ontogenies from longitudinal sequencing of B cell transcripts. *Front. Immunol.* **7**, 372 (2016). doi: [10.3389/fimmu.2016.00372](https://doi.org/10.3389/fimmu.2016.00372); pmid: [27708645](https://pubmed.ncbi.nlm.nih.gov/27708645/)
108. J. H. Ward Jr., Hierarchical grouping to optimize an objective function. *J. Am. Stat. Assoc.* **58**, 236–244 (1963). doi: [10.1080/01621459.1963.10500845](https://doi.org/10.1080/01621459.1963.10500845)
109. R. W. Sanders et al., A next-generation cleaved, soluble HIV-1 Env trimer, BG505 SOSIP.664 gp140, expresses multiple epitopes for broadly neutralizing but not non-neutralizing antibodies. *PLoS Pathog.* **9**, e1003618 (2013). doi: [10.1371/journal.ppat.1003618](https://doi.org/10.1371/journal.ppat.1003618); pmid: [24068931](https://pubmed.ncbi.nlm.nih.gov/24068931/)
110. M. Pancera et al., Structure and immune recognition of trimeric pre-fusion HIV-1 Env. *Nature* **514**, 455–461 (2014). doi: [10.1038/nature13808](https://doi.org/10.1038/nature13808); pmid: [25296255](https://pubmed.ncbi.nlm.nih.gov/25296255/)
111. Y. D. Kwon et al., Surface-matrix screening identifies semi-specific interactions that improve potency of a near pan-reactive HIV-1-neutralizing antibody. *Cell Rep.* **22**, 1798–1809 (2018). doi: [10.1016/j.celrep.2018.01.023](https://doi.org/10.1016/j.celrep.2018.01.023); pmid: [29444432](https://pubmed.ncbi.nlm.nih.gov/29444432/)
112. C. Suloway et al., Automated molecular microscopy: The new Legion system. *J. Struct. Biol.* **151**, 41–60 (2005). doi: [10.1016/j.jsb.2005.03.010](https://doi.org/10.1016/j.jsb.2005.03.010); pmid: [15890530](https://pubmed.ncbi.nlm.nih.gov/15890530/)
113. N. R. Voss, C. K. Yoshioka, M. Radermacher, C. S. Potter, B. Carragher, DoG Picker and TiltPicker: Software tools to facilitate particle selection in single particle electron microscopy. *J. Struct. Biol.* **166**, 205–213 (2009). doi: [10.1016/j.jsb.2009.01.004](https://doi.org/10.1016/j.jsb.2009.01.004); pmid: [19374019](https://pubmed.ncbi.nlm.nih.gov/19374019/)
114. G. C. Lander et al., Appion: An integrated, database-driven pipeline to facilitate EM image processing. *J. Struct. Biol.* **166**, 95–102 (2009). doi: [10.1016/j.jsb.2009.01.002](https://doi.org/10.1016/j.jsb.2009.01.002); pmid: [19263523](https://pubmed.ncbi.nlm.nih.gov/19263523/)
115. S. Q. Zheng et al., MotionCor2: Anisotropic correction of beam-induced motion for improved cryo-electron microscopy. *Nat. Methods* **14**, 331–332 (2017). doi: [10.1038/nmeth.4193](https://doi.org/10.1038/nmeth.4193); pmid: [28250466](https://pubmed.ncbi.nlm.nih.gov/28250466/)
116. A. Rohou, N. Grigorieff, CTFIND4: Fast and accurate defocus estimation from electron micrographs. *J. Struct. Biol.* **192**, 216–221 (2015). doi: [10.1016/j.jsb.2015.08.008](https://doi.org/10.1016/j.jsb.2015.08.008); pmid: [26278980](https://pubmed.ncbi.nlm.nih.gov/26278980/)
117. K. Zhang, Gctf: Real-time CTF determination and correction. *J. Struct. Biol.* **193**, 1–12 (2016). doi: [10.1016/j.jsb.2015.11.003](https://doi.org/10.1016/j.jsb.2015.11.003); pmid: [26592709](https://pubmed.ncbi.nlm.nih.gov/26592709/)
118. S. H. Scheres, RELION: Implementation of a Bayesian approach to cryo-EM structure determination. *J. Struct. Biol.* **180**, 519–530 (2012). doi: [10.1016/j.jsb.2012.09.006](https://doi.org/10.1016/j.jsb.2012.09.006); pmid: [23000701](https://pubmed.ncbi.nlm.nih.gov/23000701/)

119. A. Punjani, J. L. Rubinstein, D. J. Fleet, M. A. Brubaker, cryoSPARC: Algorithms for rapid unsupervised cryo-EM structure determination. *Nat. Methods* **14**, 290–296 (2017). doi: [10.1038/nmeth.4169](https://doi.org/10.1038/nmeth.4169); pmid: [28165473](https://pubmed.ncbi.nlm.nih.gov/28165473/)
120. Q. Liu *et al.*, Improvement of antibody functionality by structure-guided paratope engraftment. *Nat. Commun.* **10**, 721 (2019). doi: [10.1038/s41467-019-08658-4](https://doi.org/10.1038/s41467-019-08658-4); pmid: [30760721](https://pubmed.ncbi.nlm.nih.gov/30760721/)
121. P. D. Adams *et al.*, Recent developments in the PHENIX software for automated crystallographic structure determination. *J. Synchrotron Radiat.* **11**, 53–55 (2004). doi: [10.1107/S0909049503024130](https://doi.org/10.1107/S0909049503024130); pmid: [14646133](https://pubmed.ncbi.nlm.nih.gov/14646133/)
122. P. Emsley, K. Cowtan, Coot: Model-building tools for molecular graphics. *Acta Crystallogr. D* **60**, 2126–2132 (2004). doi: [10.1107/S0907444904019158](https://doi.org/10.1107/S0907444904019158); pmid: [15572765](https://pubmed.ncbi.nlm.nih.gov/15572765/)
123. I. W. Davis, L. W. Murray, J. S. Richardson, D. C. Richardson, MOLPROBITY: Structure validation and all-atom contact analysis for nucleic acids and their complexes. *Nucleic Acids Res.* **32** (suppl. 2), W615–W619 (2004). doi: [10.1093/nar/gkh398](https://doi.org/10.1093/nar/gkh398); pmid: [15215462](https://pubmed.ncbi.nlm.nih.gov/15215462/)
124. B. A. Barad *et al.*, EMRinger: Side chain-directed model and map validation for 3D cryo-electron microscopy. *Nat. Methods* **12**, 943–946 (2015). doi: [10.1038/nmeth.3541](https://doi.org/10.1038/nmeth.3541); pmid: [26280328](https://pubmed.ncbi.nlm.nih.gov/26280328/)
125. D. Fera *et al.*, Affinity maturation in an HIV broadly neutralizing B-cell lineage through reorientation of variable domains. *Proc. Natl. Acad. Sci. U.S.A.* **111**, 10275–10280 (2014). doi: [10.1073/pnas.1409954111](https://doi.org/10.1073/pnas.1409954111); pmid: [24982157](https://pubmed.ncbi.nlm.nih.gov/24982157/)
126. W. Kabsch, XDS. *Acta Crystallogr. D* **66**, 125–132 (2010). doi: [10.1107/S0907444909047337](https://doi.org/10.1107/S0907444909047337); pmid: [20124692](https://pubmed.ncbi.nlm.nih.gov/20124692/)
127. A. J. McCoy *et al.*, Phaser crystallographic software. *J. Appl. Crystallogr.* **40**, 658–674 (2007). doi: [10.1107/S0021889807021206](https://doi.org/10.1107/S0021889807021206); pmid: [19461840](https://pubmed.ncbi.nlm.nih.gov/19461840/)
128. P. Emsley, B. Lohkamp, W. G. Scott, K. Cowtan, Features and development of Coot. *Acta Crystallogr. D* **66**, 486–501 (2010). doi: [10.1107/S0907444910007493](https://doi.org/10.1107/S0907444910007493); pmid: [20383002](https://pubmed.ncbi.nlm.nih.gov/20383002/)
129. G. Tang *et al.*, EMAN2: An extensible image processing suite for electron microscopy. *J. Struct. Biol.* **157**, 38–46 (2007). doi: [10.1016/j.jsb.2006.05.009](https://doi.org/10.1016/j.jsb.2006.05.009); pmid: [16859925](https://pubmed.ncbi.nlm.nih.gov/16859925/)
130. F. K. Treurnicht *et al.*, Adaptive changes in HIV-1 subtype C proteins during early infection are driven by changes in

- HLA-associated immune pressure. *Virology* **396**, 213–225 (2010). doi: [10.1016/j.virol.2009.10.002](https://doi.org/10.1016/j.virol.2009.10.002); pmid: [19913270](https://pubmed.ncbi.nlm.nih.gov/19913270/)
131. R. Andrabi *et al.*, The chimpanzee SIV envelope trimer: Structure and deployment as an HIV vaccine template. *Cell Rep.* **27**, 2426–2441.e6 (2019). doi: [10.1016/j.celrep.2019.04.082](https://doi.org/10.1016/j.celrep.2019.04.082); pmid: [31116986](https://pubmed.ncbi.nlm.nih.gov/31116986/)

ACKNOWLEDGMENTS

We thank A. Abuahmad, H. Chen, A. Eaton, A. Foulger, M. Gladden, T. Gurley, G. Hernandez, A. Huang, C. Jones, J. Kim, J. Meyer, A. Monroe, R. Parks, A. Ransier, J. Rathmann, P. Rawls, A. Sanzone, J. Spreng, K. Tilahun, R. Verardi, T. Von Holle, A. Wang, and R. Zhang for technical assistance and the flow cytometry core staff at the Duke Human Vaccine Institute and NIAID/NIH Vaccine Research Center. We thank T. Denny, T. Demarco, and N. DeNaeyer and members of the Nonhuman Primate Virology Core Laboratory at the Duke Human Vaccine Institute for SHIV plasma vRNA measurements, and J. Baalwa, D. Ellenberger, F. Gao, K. Hong, F. McCutchan, D. Montefiori, L. Morris, J. Overbaugh, E. Sanders-Buell, R. Swanstrom, M. Thomson, S. Tovanabutra, C. Williamson, and L. Zhang for contributing HIV-1 Env plasmids. We thank K. McKee, C. Moore, S. O'Dell, G. Padilla, S. D. Schmidt, C. Whittaker, A. B. McDermott, and M. Seaman for assistance with neutralization assays, D. Fera for helpful advice and discussion, and the staff at Bioqual for exceptional care and assistance with nonhuman primates. Cryo-EM was performed at the Simons Electron Microscopy Center and National Resource for Automated Molecular Microscopy located at the New York Structural Biology Center and was supported by grants from the Simons Foundation (SF349247), NYSTAR, and the NIH National Institute of General Medical Sciences GM103310. X-ray diffraction data were collected on the Northeastern Collaborative Access Team beamline 24 ID-C (Advanced Photon Source). **Funding:** This work was funded by the Bill and Melinda Gates Foundation (OPP1145046 and OPP1206647/INV-007939); by the Intramural Research Program of the NIAID/NIH Vaccine Research Center; and by the Division of AIDS (NIAID/NIH) through support of the Duke Center for HIV/AIDS Vaccine Immunology-Immunogen Discovery (UM1 AI100645), the Duke Consortium for HIV/AIDS Vaccine Development (UM1 AI144371), the Penn Center for AIDS Research (P30 AI045008), and grants AI131251, AI131331, AI128832, AI050529, AI150590, and

AI140897. R.S.R. was supported by an NIH training grant in HIV pathogenesis (T32-AI007632). X-ray diffraction data were funded by NIH grant P41 GM103403. **Author contributions:** Conceptualization: G.M.S., B.H.H., S.C.H., B.T.K., P.D.K., J.R.M., G.K., M.R., D.C.D., H.L., and R.S.R. Investigation and data analysis: R.S.R., H.L., W.B.W., H.C., R.D.M., J.G., S.W., F.-H.L., J.R., M.B., K.-K.H., K.O.S., K.Wi., M.A.M., P.T.H., K.Wa., E.E.G., R.M.R., F.B.-R., W.L., J.C., A.G.S., J.D., A.I.M., J.S., W.D., C.Z., N.C., M.O., C.R., Y.D., E.L., A.M.B., K.J.B., D.A., C.W.C., G.-Y.C., H.G., B.C.L., M.K.L., R.N., B.Z., M.G.L., D.D.R., N.A.D.-R., C.A.S., D.C.D., M.R., T.B.K., G.K., J.R.M., P.D.K., B.T.K., S.C.H., B.F.H., B.H.H., and G.M.S. Writing – original draft: G.M.S., R.S.R., W.B.W., B.T.K., H.C., S.C.H., and P.D.K. Writing – review, editing, and approval: all authors. **Competing interests:** The authors do not have any competing interests. **Data and materials availability:** Sequencing data are available from GenBank: MN471655-MN472016, MT484339-MT487491, MT580365-MT580445, MT509359, GQ999989, HQ625604, KC863461-KC863464, KF241776, KF996577-KF996601, KF996604, KF996606, KF996610-KF996630, KF996632-KF996662, KF996664-KF996678, KF996680, KF996682-KF996683, KF996685-KF996716, KT698223-KT698227, MF572809-MF572829, EF203980-EF203981, MK205498-MK205507, MT581213-MT581268, MT610888-MT610895, and MT656172-MT656253. Cryo-EM maps and fitted coordinates have been deposited with database codes EMDB-22295 and PDB ID 6XRT, respectively. DH650 bound to the gp120 core was deposited with database code PDB ID 6XCJ.

SUPPLEMENTARY MATERIALS

science.sciencemag.org/content/371/6525/eabd2638/suppl/DC1
Supplementary Text
Figs. S1 to S27
Tables S1 to S6
References (132–136)
MDAR Reproducibility Checklist
[View/request a protocol for this paper from Bio-protocol.](https://www.biorxiv.org/content/10.1101/2020.06.10.354921)

10 June 2020; accepted 9 November 2020
Published online 19 November 2020
[10.1126/science.abd2638](https://doi.org/10.1126/science.abd2638)

Recapitulation of HIV-1 Env-antibody coevolution in macaques leading to neutralization breadth

Ryan S. RoarkHui LiWilton B. WilliamsHema ChugRosemarie D. MasonJason GormanShuyi WangFang-Hua LeeJuliette RandoMattia BonsignoriKwan-Ki HwangKevin O. SaundersKevin WieheM. Anthony MoodyPeter T. HraberKshitij WaghElena E. GiorgiRonnie M. RussellFrederic Bibollet-RucheWeimin LiuJesse ConnellAndrew G. SmithJulia DeVotoAlexander I. MurphyJessica SmithWenge DingChengyan ZhaoNeha ChohanMaho OkumuraChristina RosarioYu DingEmily LindemuthAnyam M. BauerKatharine J. BarDavid AmbrozakCara W. ChaoGwo-Yu ChuangHui GengBob C. LinMark K. LouderRichard NguyenBaoshan ZhangMark G. LewisDonald D. RaymondNicole A. Doria-RoseChaim A. SchrammDaniel C. DouekMario RoedererThomas B. KeplerGarnett KelsoeJohn R. MascolaPeter D. KwongBette T. KorberStephen C. HarrisonBarton F. HaynesBeatrice H. HahnGeorge M. Shaw

Science, 371 (6525), eabd2638.

Convergent HIV evolution across species

Human immunodeficiency virus (HIV) has a highly diverse envelope protein that it uses to target human cells, and the complexity of the viral envelope has stymied vaccine development. Roark *et al.* report that the immediate and short-term evolutionary potential of the HIV envelope is constrained because of a number of essential functions, including antibody escape. Consequently, when introduced into humans as HIV or into rhesus macaque monkeys as chimeric simian-human immunodeficiency virus, homologous envelope glycoproteins appear to exhibit conserved patterns of sequence evolution, in some cases eliciting broadly neutralizing antibodies in both hosts. Conserved patterns of envelope variation and homologous B cell responses in humans and monkeys represent examples of convergent evolution that may serve to guide HIV vaccine development.

Science, this issue p. eabd2638

View the article online

<https://www.science.org/doi/10.1126/science.abd2638>

Permissions

<https://www.science.org/help/reprints-and-permissions>

Use of think article is subject to the [Terms of service](#)